이학박사학위논문

Dual-eGRASP 기술을 이용한 해마 및 편도에서의 기억 저장 시냅스 연구

Studies on synaptic engram in hippocampus and amygdala using Dual-eGRASP

2020년 8월

서울대학교 대학원

뇌과학전공

최 동 일

ABSTRACT

Studies on synaptic engram in hippocampus and amygdala using Dual-eGRASP

Dong Il Choi

School of Brain Science

The Graduate School

Seoul National University

Our daily experiences are stored in the brain as form of memories and define one person's individuality. It has long been human being’s interests, where and how the memory is encoded in our brain. In this acquisition and storage process of memories, structural and physiological changes occur, which is considered as the physical substrates of the memory or the engram. During the memory formation, synapses between neurons undergo plasticity. Neurobiologists have tried to observe these changes in the synapses between engram cells. However, substrate at synapse-level within engram cells remains elusive, because of technical limitations. To distinguish the connections between engram cell and other neurons, I developed and applied dual-eGRASP technique.

Using Dual-eGRASP, I could capture the “Synaptic engrams” in the hippocampus and amygdala, which are the connections between pre- and post-

synaptic engram cells among intermingled neuronal ensembles. Tracking the synaptic engram in hippocampus CA3 to CA1 Schaffer-collateral pathway, I found the strength of memory is correlated with density and spine size of synaptic engrams, not depend on number of engram cells. Moreover, in the lateral amygdala (LA), I found that extinction of fear memory reversed the synaptic enhancement induced by fear conditioning. In addition, re-conditioning with same tone and shock recovered the spine size of synaptic engram decreased by fear extinction. These results indicate that the connections between engram cells, synaptic engram, represents the state of memory. These synaptic-level engram approaches will provide information on the question, “how the memory is encoded in our brain.”

.....

Keywords : Memory, Engram, Hippocampus, Amygdala, Extinction, Dual-eGRASP

Student Number : 2015-22682

CONTENTS

LIST OF FIGURES

CHAPTER I

INTRODUCTION

BACKGROUND

Learning and memory is a key component of cognition. Our daily experience is retained as memory, constituting the individual's character. It has long been human being's interest "How can memory be encoded in our brain?" Most of previous studies have been focused on the molecular, cellular and physiological changes after memory formation. However, while these studies explain the mechanisms of memory encoding, the physical substrates of memory called "engram" are still elusive. Furthermore, despite the advancements in techniques, most of the previous studies are limited in neuronal level in engram approach since there were no proper tools to distinguish the connections between engram cells and non-engram cells.

Associated fear conditioning

To artificially mimic the declarative memory, associated fear learning test has been widely used. Two major fear learning task, auditory fear condition (AFC) and contextual fear conditioning (CFC), have been conducted for measuring the episodic memory (Fanselow, 2000). AFC pairs the neutral auditory stimulus with aversive foot shock, while CFC associate the contextual cue with aversive stimulus. Re-exposure of neutral stimulus without aversive stimulus could evoke the fear response shown as "freezing" (a time spent with immobile) phenotype. Throughout measuring the time of fear response, we could examine whether fear memory has formed (Fig 1).

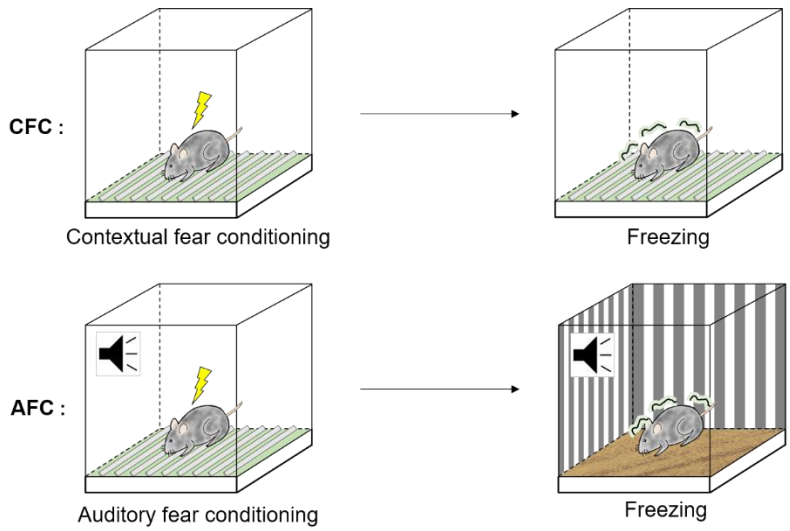

Figure 1. Schematic illustration of associated fear learning (CFC and AFC).

(A) Contextual fear conditioning; mouse was exposed into a context and given electric shocks. After fear association process, the mouse showed immobile behavior (freezing) when it exposed to the same context.

(B) Auditory fear conditioning; mouse was placed in the context, followed by exposure of auditory tone, co-terminated with aversive electric foot shock. After, fear association with tone and shock, the mouse showed freezing when it exposed to the same tone.

Hippocampus

Hippocampus, the part of the limbic system, is located deep into temporal lobe. This separated subregion is highly conserved throughout evolutionary process. Because, this structure is a key component for encoding and expressing the episodic memory in vertebrates, it is crucial for survival. Hippocampus is composed of several subregions; Cornu Ammonis (CA)1, CA2, CA3, dentate gyrus (DG) and Hilus. Numerous studies have been conducted, including anatomical and structural approaches, as well as electrophysiological character screening and LTP inductions. Importance roles in memory process and relatively easy to access, the hippocampus is appropriate brain region for studying the mechanism of memory encoding.

Amygdala

Amygdala, also the component of the limbic system, is a collection of nuclei located deep within the temporal lobe. The term of amygdala originates from Latin word “almond”, because major part of amygdala nuclei has almond like structure. Amygdala is as important as hippocampus for the survival of animals, because of it roles in encoding the emotions and related behavior. The amygdala nuclei consist of several subregions including lateral amygdala (LA), basolateral Amygdala (BLA), central amaygdala (CeA) and intercalating cell mass (ITC). Their detailed roles are slightly different, but are commonly related to emotional balance and formation of episodic memory. Especially, LA is well known region for receiving the thalamic and cortical inputs, in which associates the unconditioned stimulus (US) and conditioned stimulus (CS) in classical fear conditioning.

Immediate early gene

Immediate early genes (IEG) are a class of genes that rapidly but transiently are expressed in activated cell. More than 100 types of IEGs have been classified, but only a few have been identified in neurons (Minatohara et al., 2016; Sheng and Greenberg, 1990). The most common IEGs expressed in neurons are *Arc, Zif268,* and *c-Fos*, but their exact roles are still controversial (Lyford et al., 1995; Maleeva et al., 1989). Interestingly, neurons labeled with various types of IEG are not always co-expressed at high levels (Minatohara et al., 2016). Each gene represents neuronal activity, although with different expression times and roles. Nevertheless, c-Fos is the most representative IEG and commonly used gene for engram cell marking (Abdou et al., 2018; Liu et al., 2012; Pignatelli et al., 2019).

Engram

Richard W. Semon introduced the term "Engram" to describe the physical substrate of the memory (Semon, 1921, 1923). Specific populations of neurons that are activated during the memory acquisition undergo physical and physiological changes and are allocated as engram. The memory engram among complex neuronal ensembles, has necessity and sufficiency condition for memory expression. The quest to identify the memory engram, and the specific sites of memory storage, has been remained as goal in the neuroscience field. The early attempts to find the physical evidence of memory, engram, was crude and unsuccessful due to technical limitations. However, with the advancement of engram tagging and manipulation techniques, studies on memory storage and expression mechanisms have come to a transition (Deng et al., 2013; Reijmers et al., 2007; Xie et al., 2014). Immediate early

gene based engram tagging allows identification of engram ensembles in several brain regions associated with various behaviors and memories. Also, using new powerful techniques such as Designer Receptors Exclusively Activated by Designer Drugs (DREADD) and optogenetics allowed that modulate specific populations of neurons. Through activation or inhibition of specific population of cells, it has been revealed that engrams are crucial for memory formation and expression. Thus, it is widely accepted that these specific neuronal populations comprise the engram (Josselyn et al., 2015; Josselyn and Tonegawa, 2020).

The historical experiment to prove the sufficiency of the engram cell was performed by Tonegawa group using a Fos-tTA engram tagging system and optogenetics (Liu et al., 2012). Activated hippocampal dentate gyrus neurons during fear memory acquisition became the engram cells that encode contextual memory. The stimulation of these selective dentate gyrus engram cells could elicit the fear response, even in the novel context. After this report, many engram studies have been conducted in the last decade for demonstrating the necessity and sufficiency of engram cells (Gore et al., 2015; Ryan et al., 2015)..

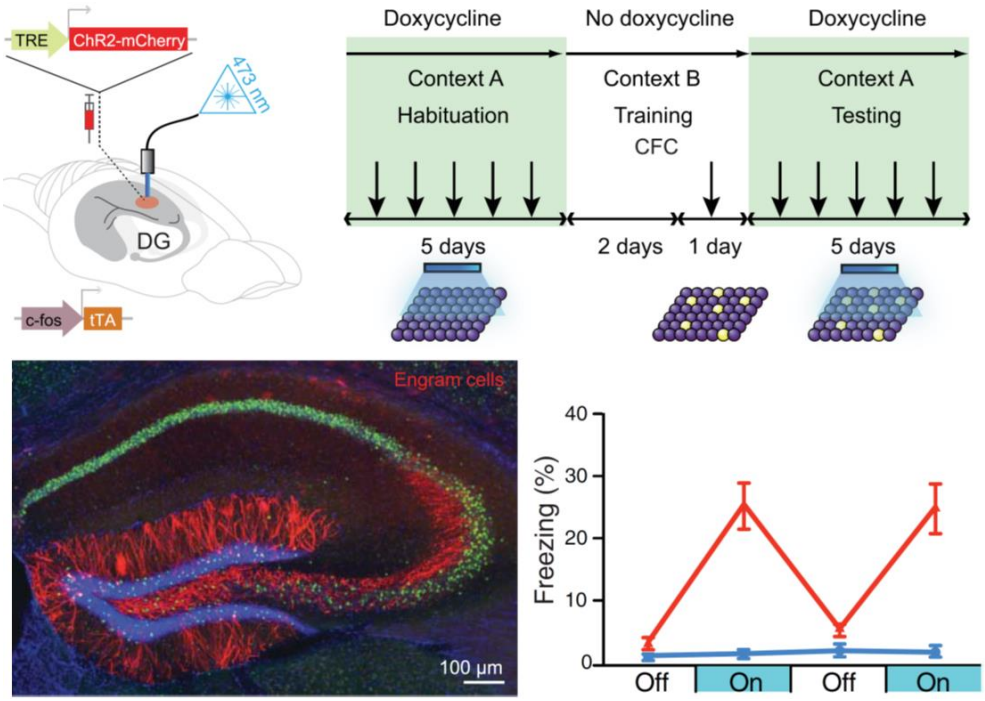

(Adapted from Josselyn and Tonegawa, 2020)

Figure 2. Demonstration of engram cell.

Basic experimental scheme of engram cell reactivation. Activated dentate gyrus neurons during fear conditioning became the engram cells that encode contextual memory. Optogenetical stimulation of these engram cells could elicit the fear response, even in the novel context.

Dual-eGRASP

To label the synapse between two neurons, the new technique, green fluorescent protein reconstitution across synaptic partners (GRASP), was introduced (Feinberg et al., 2008; Kim et al., 2011). GRASP uses two complementary mutant GFP fragments. These fragments are separately expressed on the presynaptic and postsynaptic membrane and reconstitute in the synaptic cleft to form functional GFP. This GFP signal indicates the synapse formed between the neurons expressing the presynaptic component and the neuron expressing the postsynaptic component. However, the conventional GRASP signal was too weak and only could capture the one kind of synapse with green color. To overcome these limitations, dual-eGRASP was invented.

Increasing GRASP signal intensity throughout changing of interacting domain, which is facilitates by reconstitution of GFP and a single mutation commonly found on most advanced GFP variants. Additionally, cyan- and yellow-eGRASP were introduced by a series of rationally selected mutations. The color-determining domain was placed on the presynaptic neuron (cyan/yellow pre-eGRASP) and the common domain to the postsynaptic neuron (post-eGRASP). This enables visualize the two synaptic populations that originated from two different presynaptic neuron populations projected to a single postsynaptic neuron. Through these two advances, dual-eGRASP can label various synapses in two different colors with enhanced fluorescence (Choi et al., 2018).

PURPOSE OF THIS STUDY

The “Engram”, physical substrate of memory, has been spotlighted in recent decade. Recently, thanks for advancement of neuronal marking and manipulation technique, structural and physiological properties of engram cell had been vigorously researched. Now we know, neuronal ensembles which show higher excitability during memory formation are allocated as engram, and those are re-activated for expression of memory. It implicates that recent studies have succeeded to identifying and manipulating of the memory engram in various brain regions. Despite these achievements, previous studies had limitations in studying essence of the engram, which is synaptic-level engram approach. The synapses between engrams are required to be more focused for understanding the nature of memory, because synapse is a functional unit of our nervous system. In this thesis, I identified synaptic engrams in various brain region using dual-eGRASP, and demonstrated that “synaptic engram represents the different state of memory.”

In chapter II, I applied dual-eGRASP to identify the synaptic engrams in hippocampus and amygdala, in which are well known for encoding the episodic memory. Dual-eGRASP could distinguish four kinds of synaptic combinations between engrams and non-engrams (engram to engram, engram to non-engram, non-engram to engram, non-engram to non-engram), and I defined the synapses between the engrams as “synaptic engram.” Synaptic engrams in the hippocampus encodes the contextual information, where as in lateral amygdala, unconditioned and conditioned stimuli are associated at synaptic engram. Throughout labeling the synaptic engrams, I could trace the physical evidence of memory after fear conditioning.

In chapter III, I analyzed the synaptic engrams in mice hippocampus schaffer collateral pathway. I quantified the number of CA3 and CA1 engram cells across three different memory intensity groups. Next, I measured the synaptic density and spine morphology of E-E spine to reveal the co-relations between synaptic engram and memory intensity.

In chapter IV, I labeled the synapses between cortico-amygdala engram neurons and compared the morphological dynamics after fear learning, extinction and re-conditioning. Subsequently, I investigated whether extinction and re-conditioning recruit distinct neuronal ensembles from the original fear engram neurons that drive auditory fear memories in LA and AC, or it changes the previous formed synaptic engram.

Collectively, in this thesis, I identified the synaptic engram in various regions using dual-eGRASP. Furthermore, I traced the memory encoding spines to demonstrate whether synaptic engram represent the various state of memory.

CHAPTER II

Identification of synaptic engram using Dual-eGRASP

INTRODUCTION

Our daily experiences are stored in the brain as memories and they define one person's individuality. In these acquisition and storage of memories, structural and physiological changes occur in various areas in the brain. In 1904, Richard Semon coined the term 'Engram' to define the physical changes during the memory formation. This Engram is roughly considered as a "trace of memory". Recently, thanks for the development of fluorescence tagging system and cell specific modulation tool, the evidence of engram cells has been solidified, which has been accepted as a truth. Despite these advances, however, most of the researches has been conducted at the neuronal level rather than the synapse levels. It was because there were no proper tools for distinguishing different synaptic populations which originates from specific engram neurons.

Then, we can raise the question, "Why the synaptic level approach in engram is important?" Neurons, unlike other types of cells, receive and transmit information from and to other neurons. These neuronal information relaying is occurred through the synapse, the cleft between neurons. Synapse is a structure that permits a neuron to pass an electrochemical signal to another neuron. Each synapse has its own dynamics in functional and structural aspects depending on their activity. It is known as "synaptic plasticity". Therefore, a synapse, not a neuron is a functional unit of our brain., and it had been widely studied through various research technique in various scales. Observing the synapses between engram cell is strongly emphasized to investigate the synaptic mechanism of learning and memory.

The word "synapse", meaning of conjunction, was first mentioned by

English neurophysiologist Charles Sherrington in 1897. After identification of this neuronal conjunction, many neuroscientists tried to capture the synapses. In 1955, using electron microscopy (EM), structure of synapse was revealed and remarkable information for understanding the role of synapse was provided. However, structural approaches using EM required laborious experimental procedural and time-consumptions. Nonetheless, several studies have found that dendritic spine density and morphology change with memory formation (Chen et al., 2010; Leuner et al., 2003; Matsuzaki et al., 2001; Matsuzaki et al., 2004; Sanders et al., 2012). However, it was unknown whether these structural enhancements occurred specifically at synapses between engram neurons that are activated during memory formation. To investigate synaptic level changes after memory formation, I applied recently developed synapse marking technique, the dual-eGRASP.

In this chapter, I used dual-eGRASP to capture the "synaptic engrams" in the hippocampus and amygdala, which are the connections between pre-synaptic and post-synaptic engram cells among intermingled neuronal ensembles. First, I validated of Fos-rtTA system and teto promoter based engram labeling system. Applying dual-eGRASP with Fos-rtTA, I distinguished four synaptic combinations (engram to engram, engram to non-engram, non-engram to engram, non-engram to non-engram) at hippocampus CA3 to CA1 schaffercolateral pathway and auditory cortex to lateral amygdala connections.

EXPERIMENTAL PROCEDURES

Animals

All experiments were performed on 8~12-week-old male C57BL/6N mice purchased from Samtako. Bio. Korea. Mice were raised in 12-hr light/dark cycle (8:30AM – 8:30PM) in standard laboratory cages and given ad libitum access to food and water. All procedures and animal care were followed the regulation and guidelines of the Institutional Animal Care and Use Committees (IACUC) of Seoul National University.

Construction of Fos-rtTA system

Temporally-controlled activity-dependent transgene expression used a Fos promoter driven rtTA3G with an additional AU-rich element of Fos mRNA, which induced rapid destabilization of the mRNA following the rtTA3G. The transgenes of interest were expressed by a TRE3G promoter, in the presence of both rtTA3G protein and doxycycline.

Construction of cyan and yellow eGRASP

The pre-eGRASP construct consists with an IgG kappa signal peptide, strand 1-10 of the mutant GFP, an Abl SH3 binding peptide, and a neurexin1b stalk, transmembrane and intracellular domain. The strand 1-10 contains an S72A (amino acid numbering based on GFP sequence) mutation additionally to the original GRASP mutations. The cyan pre-eGRASP contains additional T65S, Y66W, H148G, T205S mutations including the S72A mutation, while yellow pre-eGRASP contains

S72A and T203Y mutations. The Abl SH3 binding peptide was either p30 (APTKPPPLPP) or p32 (SPSYSPPPPP). The post-eGRASP construct consists with an IgG kappa signal peptide, an Abl SH3 domain, strand 11 of the mutant GFP, and a neuroligin1 stalk, transmembrane and intracellular domain with the last 4 amino acids deleted. The last 4 amino acids of the neuroligin1 which consist the PDZ domain binding site was deleted to avoid undesired recruitment of scaffolding proteins and receptors. The protein sequence of each construct is listed below.

pre-eGRASP(p30) : IgG kappa signal peptide (orange), strand 1-10 with S72A muation (green with green highlight for S72A), p30 (red), neurexin1b stalk, transmembrane and intracellular domain (blue). (p32 version has a replacement of APTKPPPLPP to SPSYSPPPPP)

METDTLLLWVLLLWVPGSTGDAPVGGSKGEELFTGVVPILVELDGDVNGH
KFSVRGEGEGDATIGKLTLKFICTTGKLPVPWPTLVTTLTYGVQCFARYPD
HMKRHDFFKSAMPEGYVQERTISFKDDGKYKTRAVVKFEGDTLVNRIELK
GTDFKEDGNILGHKLEYNFNSHNVYITADKQKNGIKANFTVRHNVEDGSV
QLADHYQQNTPIGDGPVLLPDNHYLSTQTVLSKDPNEKTGGSGGSGGSRA
PTKPPPLPPGGGSGGGSGTEVPSSMTTESTATAMQSEMSTSIMETTTTLATS
TARRGKPPTKEPISQTTDDILVASAECPSDDEDIDPCEPSSGGLANPTRVGG
REPYPGSAEVIRESSSTTGMVVGIVAAAALCILILLYAMYKYRNRDEGSYH
VDESRNYISNSAQSNGAVVKEKQPSSAKSANKNKKNKDKEYYV

Cyan pre-eGRASP(p30) : IgG kappa signal peptide (orange), strand 1-10 with mutations (green with cyan highlights for cyan-specific mutated amino acids), p30 (red), neurexin1b stalk, transmembrane and intracellular domain (blue). (p32 version has a replacement of APTKPPPLPP to SPSYSPPPPP)

METDTLLLWVLLLWVPGSTGDAPVGGSKGEELFTGVVPILVELDGDVNGH
KFSVRGEGEGDATIGKLTLKFICTTGKLPVPWPTLVTTLSWGVQCFARYPD
HMKRHDFFKSAMPEGYVQERTISFKDDGKYKTRAVVKFEGDTLVNRIELK
GTDFKEDGNILGHKLEYNFNSGNVYITADKQKNGIKANFTVRHNVEDGSV
QLADHYQQNTPIGDGPVLLPDNHYLSTQSVLSKDPNEKTGGSGGSGGSRA
PTKPPPLPPGGGSGGGSGTEVPSSMTTESTATAMQSEMSTSIMETTTTLATS
TARRGKPPTKEPISQTTDDILVASAECPSDDEDIDPCEPSSGGLANPTRVGG
REPYPGSAEVIRESSSTTGMVVGIVAAAALCILILLYAMYKYRNRDEGSYH
VDESRNYISNSAQSNGAVVKEKQPSSAKSANKNKKNKDKEYYV

Yellow pre-eGRASP(p30) : IgG kappa signal peptide (orange), strand 1-10 with mutations (green with Yellow highlights for yellow-specific mutated amino acid), p30 (red), neurexin1b stalk, transmembrane and intracellular domain (blue). (p32 version has a replacement of APTKPPPLPP to SPSYSPPPPP)

METDTLLLWVLLLWVPGSTGDAPVGGSKGEELFTGVVPILVELDGDVNGH
KFSVRGEGEGDATIGKLTLKFICTTGKLPVPWPTLVTTLTYGVQCFARYPD
HMKRHDFFKSAMPEGYVQERTISFKDDGKYKTRAVVKFEGDTLVNRIELK
GTDFKEDGNILGHKLEYNFNSHNVYITADKQKNGIKANFTVRHNVEDGSV
QLADHYQQNTPIGDGPVLLPDNHYLSYQTVLSKDPNEKTGGSGGSGGSRA
PTKPPPLPPGGGSGGGSGTEVPSSMTTESTATAMQSEMSTSIMETTTTLATS

TARRGKPPTKEPISQTTDDILVASAECPSDDEDIDPCEPSSGGLANPTRVGG

REPYPGSAEVIRESSSTTGMVVGIVAAAALCILILLYAMYKYRNRDEGSYH

VDESRNYISNSAQSNGAVVKEKQPSSAKSANKNKKNKDKEYYV

Post-eGRASP : IgG kappa signal peptide (orange), Abl SH3 domain (red), strand 11 (green), neuroligin1 stalk, transmembrane and intracellular domain with deletion (blue).

METDTLLLWVLLLWVPGSTGDAPVGGNDPNLFVALYDFVASGDNTLSITK

GEKLRVLGYNHNGEWCEAQTKNGQGWVPSNYITPVNSTGGGSGGGSGRD

HMVLHEYVNAAGITGGGSGGGSGTLELVPHLHNLNDISQYTSTTTKVPST

DITLRPTRKNSTPVTSAFPTAKQDDPKQQPSPFSVDQRDYSTELSVTIAVGA

SLLFLNILAFAALYYKKDKRRHDVHRRCSPQRTTTNDLTHAPEEEIMSLQM

KHTDLDHECESIHPHEVVLRTACPPDYTLAMRRSPDDIPLMTPNTITMIPNT

IPGIQPLHTFNTFTGGQNNTLPHPHPHPHSHS

AAV production

Adeno-Associated Viruses serotype 1/2 (AAV1/2; AAV particle that contains both serotype 1 and 2 capsids) were used in all the experiments. AAV1/2s were purified from HEK293T cells that were transfected with plasmids containing each expression cassette flanked by AAV2 ITRs, p5E18, p5E18-RXC1 and pAd-ΔF6 and cultured in 18 ml or 8 ml Opti-MEM (Gibco-BRL/Invitrogen, cat# 31985070) in a 150-mm or 100-mm culture dish, respectively. Four to five days after transfection, the medium containing AAV1/2 particles was collected and centrifuged at 3,000 rpm for 10 min. After 1 ml of heparin-agarose suspension (Sigma, cat#

H6508) was loaded onto a poly-prep chromatography column (Bio-Rad Laboratories, Inc. cat# 731-1550), the supernatant was loaded onto the column carefully. The column was washed by 4 ml of Buffer 4-150 (150 mM NaCl, pH4 10 mM citrate buffer) and 12 ml of Buffer 4-400 (400 mM NaCl, pH4 10 mM citrate buffer). The virus particles were eluted by 4 ml of Buffer 4-1200 (1.2 M NaCl, pH4 10 mM citrate buffer). The eluted solution was exchanged with PBS and concentrated using an Amicon Ultra-15 centrifugal filter unit (Millipore, cat# UFC910024). The titer was measured using quantitative RT-PCR.

Stereotaxic surgery

Mice (8~12 weeks) were anaesthetized with a ketamine/xylazine solution and positioned on a stereotaxic apparatus (Stoelting Co.). The virus mixture was injected into target regions through 32gauge needle with Hamilton syringe at a rate of 0.125 μl/min. Total injection volume per each sites was 0.5 μl, and a tip of the needle was positioned 0.1 mm below the target coordinate right before the injection for 2 minutes. After the injection was completed, the needle stayed in place for extra 7 minutes and was withdrawn slowly. Stereotaxic coordinates for each target sites were: CA3 (AP: -1.75/ ML: ±2.35/ DV: -2.45), CA1 (AP: -1.8/ ML: -1.45/ DV: -1.65 below from skull surface), auditory cortex (AP: -2.9/ ML: ±4.5/ DV: -3.2), auditory thalamus (AP: -3.1/ ML: ±1.8/ DV: -3.6), lateral amygdala (AP: -1.45/ ML: ±3.4/ DV: -4.4).

RESULTS

Dual-eGRASP can label the synapses originating from different populations.

Given the lack of tools to distinguish different connections, I overcame this challenge by exploiting our recently developed technique, dual-eGRASP, which enables selective labeling of synapses originating from specific neuronal populations. Dual-eGRASP is an intensified split fluorescent protein, which can only emit fluorescence when pre- and post-synaptic eGRASP are physically attached (Fig. 3A).

Dual-eGRASP provides us a way to distinguish the synapses according to their presynaptic neurons. Distinguishing between and comparing synapses on one dendrite makes it possible to do many things that were not previously possible (Fig. 3A). Firstly, I can compare the synapses input from two different regions projecting to one region (Fig. 3B, *left*). For example, dual-eGRASP successfully labeled synapses on one LA neuron originating from its two major inputs, AC and auditory thalamus (AT) (Fig. 4). Moreover, synapses could be classified in a cell-type-specific manner (Fig. 3B, *center*). Combinatorial expressions between dual-eGRASP and genetic tools to distinguish many cell-types, such as Cre-recombinase transgenic mouse lines, make it possible to compare the synaptic distributions from different cell-types (Fig. 5). Additionally, dual-eGRASP can compare the dynamic changes of spines after various stimuli according to the properties of presynaptic and postsynaptic neurons (Fig. 3B, *right*).

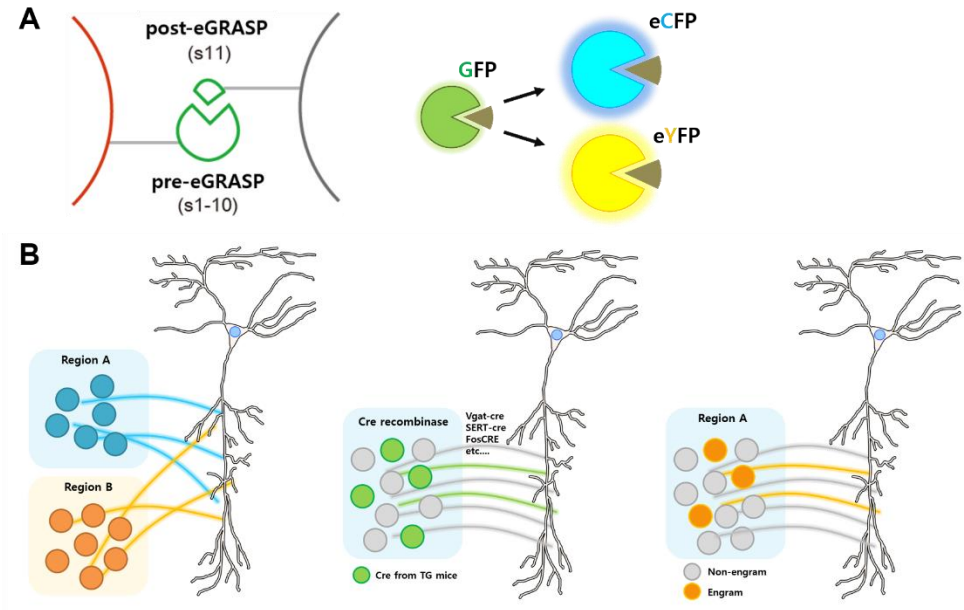

Figure 3. Dual-eGRASP could be applied to various synaptic level approach.

(A) Dual-eGRASP emit the enhanced cyan and yellow fluorescent when pre- and post-eGRASP proteins interact with other.

(B) Dual-eGRASP can distinguish the connections originating from different brain region (Left). It can label synapses between specific cell-types by using different Cre-recombinase transgenic (TG) mouse lines (Center). It can separate different neuronal projections, such as engrams in the same brain area (Right).

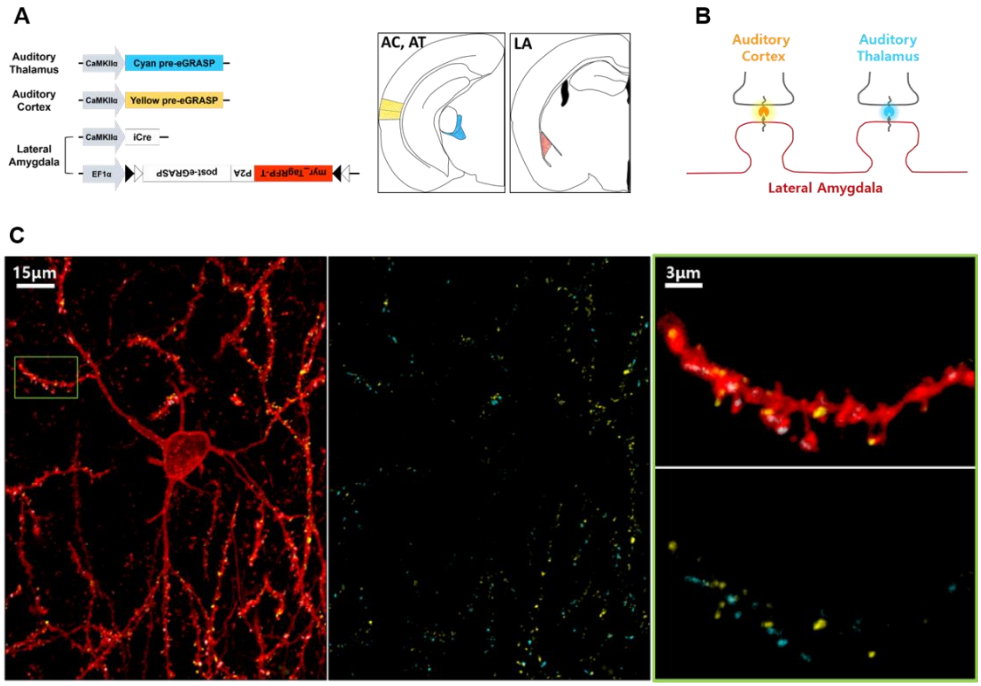

Figure 4. Dual-eGRASP differentially labels synapses on a single lateral amygdala neuron depending on their inputs.

(A) (Left) Schematics of injected virus combinations. (Right) Illustration of virus injection sites.

(B) Illustration of cyan and yellow dual-eGRASP on a single dendrite of a lateral amygdala neuron. Cyan pre-eGRASP and yellow pre-eGRASP were expressed in the auditory thalamus and auditory cortex in ipsilateral part, respectively. Post-eGRASP was expressed together with myristoylated TagRFP-T (myr_TagRFP-T) in lateral amygdala.

(C) Successful differentiation of synapses input from auditory thalamus and auditory cortex on a single pyramidal neuron in lateral amygdala.

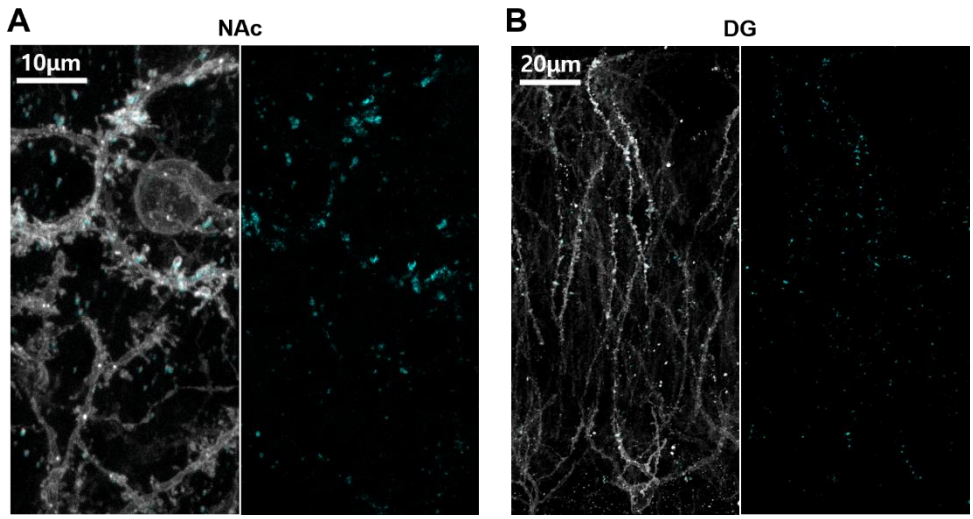

Figure 5. Dual-eGRASP label cell type specific projection combining with cre-recombinase transgenic mouse line.

(A) Illustration of dopaminergic synapses (cyan eGRASP) on nucleus accumbens (NAc) dendritic neurons, using tyrosine hydroxylase cre TG mice.

(B) Illustration of GABAergic synapses (cyan eGRASP) on dentate gyrus (DG) dendritic neurons, using somatostatin cre TG mice.

Validation of Fos-rtTA driven engram labeling system

I used a reverse tetracycline-controlled transactivator (rtTA) induced by Fos promoter to express the gene of interest in the engram cell specific manner (Haasteren et al., 2000; Loew et al., 2010; Reijmers et al., 2007; Zhou et al., 2006). Using these strategies, I can express fluorescent proteins and neuro-manipulation proteins, in any cells involved in memory acquisition, through doxycycline (Fig. 6A). To validate the Fos promoter based labeling strategy, I had confirmed whether a gene of interest could be expressed exclusively under rtTA and doxycycline. I injected the cocktail virus composed of Nucleus-targeted mEmerald (mEmerald-Nuc) driven by the TRE3G promoter which controlled by Fos promoter induced rtTA3G, and for control expression CaMKIIα driven nucleus targeted mCherry was included (Fig. 6B). I divided mice into three groups for Dox(+)/rtTA(+), Dox(+)/rtTA(-), DOX(-)/rtTA(-) and injected virus into hippocampus. Two weeks after virus injection, doxycycline was injected intraperitoneally in Dox(+) groups 2 hours before fear conditioning. As a result, only in the doxycycline and rtTA present group successfully labeled cells that activated during these memory formation (Fig. 6C).

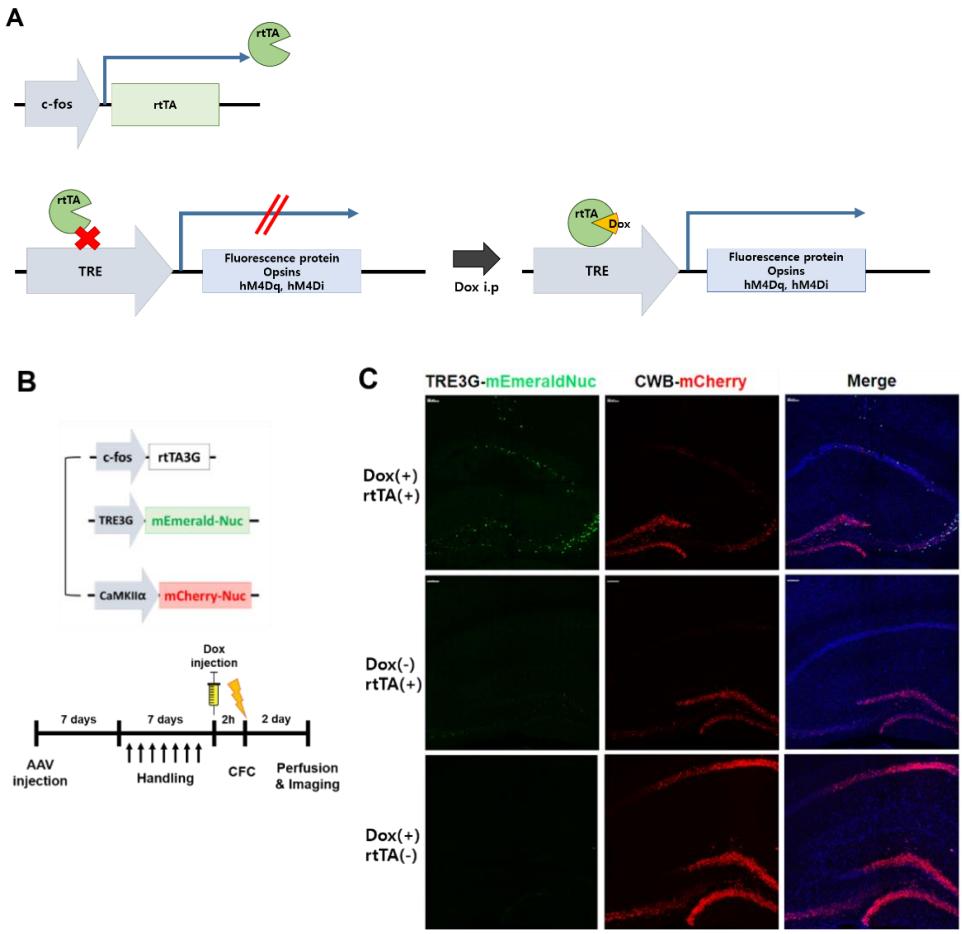

Figure 6. Validation of Fos-rtTA driven engram labeling system.

(A) Summarization of Tet tag system. rtTA proteins are expressed by c-fos promoter and transcription is induced in the presence of Dox.

(B) Schematic illustration of injected AAVs and behavioral schedule used in the experiment.

(C) Representative images of Fos-rtTA system. Fear conditioning induced a significant increase of mEmerlad-Nuc in hippocampus under present of doxycycline and rtTA.

Successful identification of the synaptic engram in hippocampus and amygdala using dual-eGRASP

Combining the dual-eGRASP with engram tagging strategy described above, I successfully discriminated four types of synapses in the same brain region after fear conditioning (Fig. 7). I captured the post-synaptic dendrites images containing distinguishable cyan and yellow eGRASP, myr_mScarlet-I (Bindels et al., 2017) and myr_iRFP670 (Shcherbakova and Verkhusha, 2013) fluorescence signals on hippocampal CA1 (Fig. 8) and lateral amygdala (Fig. 9). Cyan and yellow puncta on iRFP670 positive dendrites indicated N-N and E-N synapses, while cyan and yellow puncta on mScarlet-I positive dendrites indicated N-E and E-E synapses, respectively (Fig. 7). When the cyan and yellow eGRASP signals were overlapped in a single synapse, it was considered as a yellow spot as the presynaptic neuron of the synapse would be IEG-positive during memory formation. Above all among various synapse traces, the E-E synapses are connections only between memory encoding cells. I regarded it as synaptic map among engrams cells, the "synaptic engram".

Also I confirmed the reliability of yellow pre-eGRASP and myr_mScarlet-I expression under the Fos-rtTA system, I validated whether tetO promoter driven protein was doxycycline-dependent (Fig. 9). This result showed that this system using eGRASP technique could label synapses originating from engram cells of a specific event.

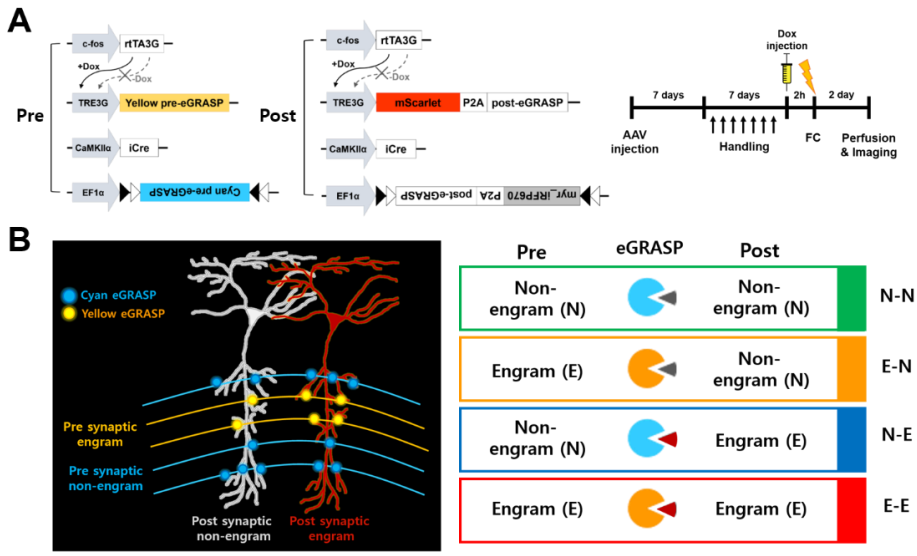

Figure 7. Virus combination and behavior scheme of synaptic engram labeling strategy.

(A) Schematic illustration of (Left) virus injected virus combinations and (Right) experimental protocol.

(B) Schematic illustration of the four possible synapse types. Cyan circles representing cyan eGRASP signals indicate synapses originating from presynaptic non-engram cells. Yellow circles representing yellow eGRASP signals indicate synapses originating from presynaptic engram cells. Postsynaptic non-engram and engram cells are shown in white and red, respectively.

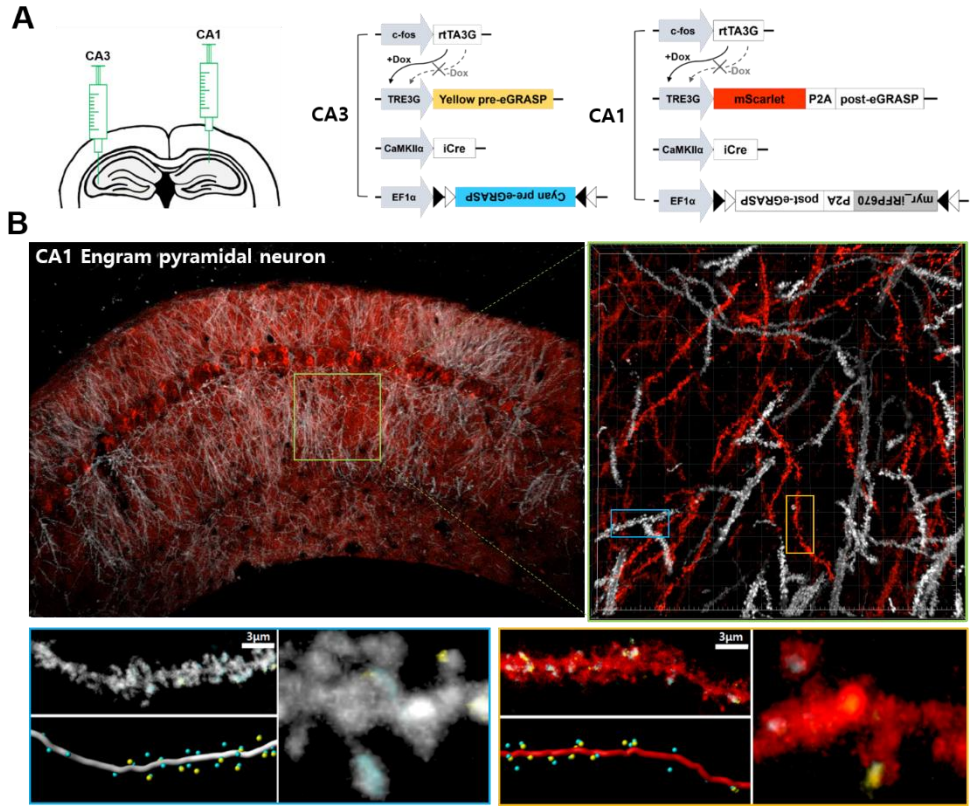

Figure 8. Identification of synaptic engram in hippocampus.

(A) Schematic illustration of virus injection sites and injected virus combinations of CA3 and CA1.

(B) (Top) Representative images of engram and non-engram dendrites with dual-eGRASP labeling in hippocampus CA1. (Bottom) Representative image of four possible synaptic combinations with three-dimensional modeling.

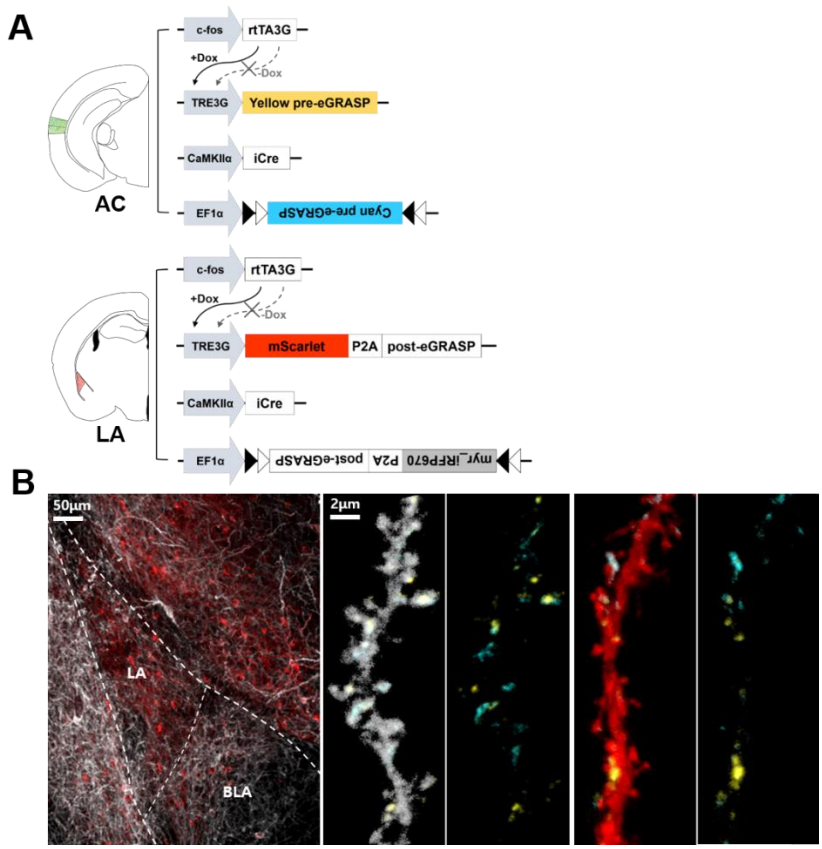

Figure 9. Identification of synaptic engram in lateral amygdala.

(A) Schematic illustration of virus injection sites and injected virus combinations of auditory cortex (AC) and lateral amygdala (LA).

(B) (Left) Representative images of engram and non-engram dendrites with dual-eGRASP labeling in lateral amygdala. (Right) Constitutive cyan dual-eGRASP signals and yellow dual-eGRASP signals expressed by conditioning.

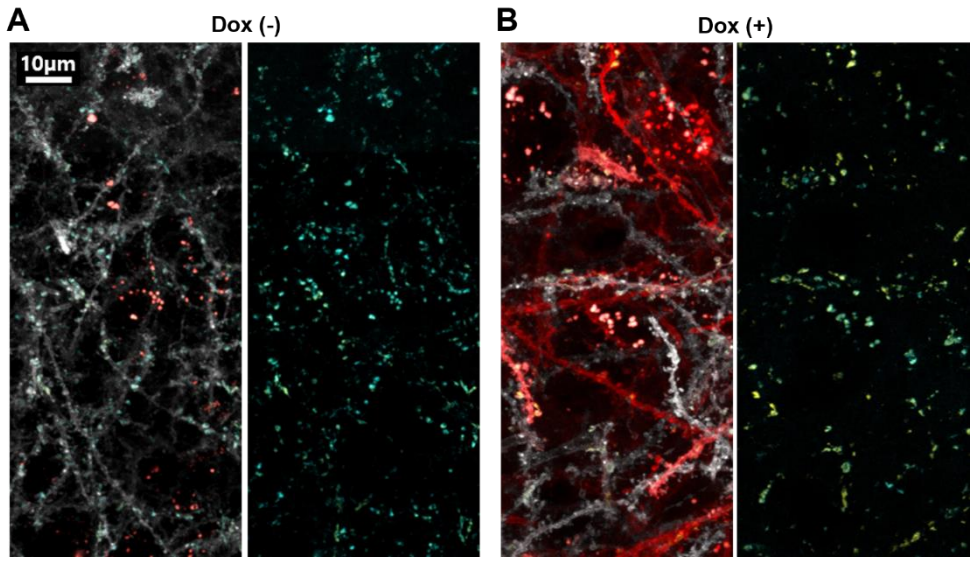

Figure 10. Validation of myr_mScarlet-i and Yellow eGRASP expression control by doxycycline.

(A and B) Representative images of dual-eGRASP construct expression without doxycycline (A) or with doxycycline injection (B).

DISCUSSION

In this chapter, I applied dual-eGRASP, to distinguish the different pre synaptic neuronal projections with cyan and yellow colors. Also, I combined this novel technique with immediate early gene based engram marking strategy, thus overcame the limitation of neuronal level engram approaches. I successfully classified four possible synapses in the hippocampus and the amygdala where engram and non-engram neurons are intermingled.

First, I showed the examples and versatility of dual-eGRASP. Distinguishing and comparing synapses on one dendrite makes it possible to do many synaptic scale studies that were not previously possible. Dual-eGRASP can compare the synapses inputs from two different regions projecting to one region. Moreover, synapses could be classified in a cell-type-specific manner. Even one brain region is consisted of various types of neurons, and each type of neuron could have a different function and connectivity. Combinatorial expressions between dual-eGRASP and genetic tools to distinguish many cell-types, such as Cre-recombinase transgenic mouse lines, make it possible to compare the synaptic distributions between different cell-types. Most of all, I could compare the dynamic changes of spines after various stimuli according to the properties of presynaptic and postsynaptic neurons. Synaptic changes are the fundamental principles of daily brain activity. Therefore, investigation of synapses affected by various stimuli is critical for understanding the basis of behavioral changes.

Observation and identification of the subject are the first step of researches, and now it is possible to observe the synaptic engrams with dual-eGRASP. I

classified some populations of synaptic ensembles that respond to episodic experiences in hippocampus and amygdala. Taken together, I could trace the change of synaptic engram, which correlates to behavioral phenotypes.

CHAPTER III

Strength of memory is correlated with density and spine size of synaptic engram

INTRODUCTION

In the previous chapter, I successfully distinguished the synaptic engrams between hippocampal CA3-CA1 schaffercolateral pathway, which encode the contextual memory. In my previous study, I found that synaptic connections originating from CA3 engram cells are predominantly innervated to CA1 post synaptic engram cells (Choi et al., 2018). Furthermore, spine size of synaptic engram was enhanced compared with other synaptic spines, after fear conditioning (Hayashi-Takagi et al., 2015; Lamprecht and LeDoux, 2004; Matsuzaki et al., 2004; Tanaka et al., 2008). These results indicate that wiring between engram cell encode the specific memory, such as contextual information in CA3 to CA1 pathway.

Even if you recall the same place, you will remember it better if you had terrible accident or if it was related to something important to you. This phenomenon appears same in the mouse fear response through contextual fear conditioning. Mice exposed in the same context with more intense electric shock could elicit strong fear response. Here I can raise the question, "Which factor determines the strength of memory?". Interestingly, previous research shows that the number of fear engram cell remain constant across different memory strengths (Morrison et al., 2016). Based on this study, we speculated that the strength of memory is depend on the connectivity between engram neurons.

In this chapter, I used dual-eGRASP to analysis the synaptic engram in CA3 to CA1 connections in three mice group of different strength of fear memory. Using Fos-rtTA based engram labeling system, I quantified the number of CA3 and

CA1 engram cells in three groups. Next, I investigated the density of connections between engram cells and measure the spine size of synaptic engrams.

EXPERIMENTAL PROCEDURES

Animals

All experiments were performed on 8~12-week-old male C57BL/6N mice purchased from Samtako. Bio. Korea. Mice were raised in 12-hr light/dark cycle (8:30AM – 8:30PM) in standard laboratory cages and given ad libitum access to food and water. All procedures and animal care were followed the regulation and guidelines of the Institutional Animal Care and Use Committees (IACUC) of Seoul National University.

Construction of Fos-rtTA system

Temporally-controlled activity-dependent transgene expression used a Fos promoter driven rtTA3G with an additional AU-rich element of Fos mRNA, which induced rapid destabilization of the mRNA following the rtTA3G. The transgenes of interest were expressed by a TRE3G promoter, in the presence of both rtTA3G protein and doxycycline.

AAV production

Adeno-Associated Viruses serotype 1/2 (AAV1/2; AAV particle that contains both serotype 1 and 2 capsids) were used in all the experiments. AAV1/2s were purified from HEK293T cells that were transfected with plasmids containing each expression cassette flanked by AAV2 ITRs, p5E18, p5E18-RXC1 and pAd-ΔF6 and cultured in 18 ml or 8 ml Opti-MEM (Gibco-BRL/Invitrogen, cat# 31985070)

in a 150-mm or 100-mm culture dish, respectively. Four days after transfection, the medium containing AAV1/2 particles was collected and centrifuged at 3,000 rpm for 10 min. After 1 ml of heparin-agarose suspension (Sigma, cat# H6508) was loaded onto a poly-prep chromatography column (Bio-Rad Laboratories, Inc. cat# 731-1550), the supernatant was loaded onto the column carefully. The column was washed by 4 ml of Buffer 4-150 (150 mM NaCl, pH4 10 mM citrate buffer) and 12 ml of Buffer 4-400 (400 mM NaCl, pH4 10 mM citrate buffer). The virus particles were eluted by 4 ml of Buffer 4-1200 (1.2 M NaCl, pH4 10 mM citrate buffer). The eluted solution was exchanged with PBS and concentrated using an Amicon Ultra-15 centrifugal filter unit (Millipore, cat# UFC910024). The titer was measured using quantitative RT-PCR.

Stereotaxic surgery

Mice (8~12 weeks) were anaesthetized with a ketamine/xylazine solution and positioned on a stereotaxic apparatus (Stoelting Co.). The virus mixture was injected into target regions through 32gauge needle with Hamilton syringe at a rate of 0.125 μl/min. Total injection volume per each sites was 0.5 μl, and a tip of the needle was positioned 0.1 mm below the target coordinate right before the injection for 2 minutes. After the injection was completed, the needle stayed in place for extra 7 minutes and was withdrawn slowly. Stereotaxic coordinates for each target sites were: CA3 (AP: -1.75/ ML: ±2.35/ DV: -2.45), CA1 (AP: -1.8/ ML: -1.45/ DV: -1.65 below from skull surface).

0.5 μl of a mixture of viruses ($1.0x10^8$ viral genome (vg)/μl of Fos-rtTA3G, $2.0x10^8$ vg/μl of TRE3G-Yellow pre-eGRASP, $4.0x10^7$ vg/μl of CaMKIIα-iCre, and $7.5x10^8$ vg/μl of EF1α-DIO-Cyan pre-eGRASP) was injected into left CA3. 0.5 μl of a mixture of viruses ($1.0x10^8$ vg/μl of Fos-rtTA3G, $8.0x10^8$ vg/μl of TRE3G-myr_mScarlet-I-P2A-post-eGRASP, $1.0x10^6$ vg/μl of CaMKIIα-iCre, $8.0x10^8$ vg/μl of EF1α-DIO-myr_iRFP670-P2A-post-eGRASP) was injected into right CA1.

Contextual fear conditioning

All behavior procedure was conducted 2 weeks after the AAV injection. Each mouse was single caged 10 days before conditioning and was habituated to the hands of the investigator for 3minutes and anesthesia chamber without isoflurane for 3 minutes on each of 7 consecutive days. Mice were conditioned 2 days after the last habituation day. On the conditioning day, 250 μl of 5 mg/ml Doxycycline solution dissolved in saline was injected by intraperitoneal injection during brief anesthesia by isoflurane in the anesthesia chamber 2 hours prior to the conditioning. Conditioning sessions to produce weak and strong memory for Figure 3 were 300 s in duration. One 0.35 mA and three 0.75 mA shocks of 2 s duration were delivered at 268 s and 208 s, 238 s, and 268 s respectively from the initiation of the session in a square chamber with a steel grid (Med Associates Inc., St Albans, VT). Mice in the context only group were exposed to the same context during 300 s. When the conditioning was finished, mice were immediately delivered to their homecage. 2 days after conditioning, mice were exposed to the same context to measure freezing levels and were carefully perfused for eGRASP signal analysis

Sample preparation and confocal imaging

Perfused brains were fixed with 4% paraformaldehyde (PFA) in PBS overnight at 4℃ and dehydrated in 30% sucrose in PBS for 2 days at 4℃. After freezing, brains were sliced into 50 μm sections by Cryostat and mounted in VECTASHIELD mounting medium (Vector Laboratories) or Easy-index mounting medium (Live Cell Instrument). CA1 apical dendritic regions of the brain slices were imaged by Leica SP8 confocal microscope with 63x objectives with distilled water immersion. Secondary/tertiary dendrites of CA1 neurons were imaged in Z-stack.

Image analysis

Imaris (Bitplane, Zurich, Switzerland) software was used to reconstruct 3D models of the confocal images. Each trackable myr_mScarlet-I-positive, myr_mScarlet-I-positive or myr_iRFP670-positive dendrite was denoted as a filament manually while hiding other three channels to exclude any bias, and each cyan or yellow eGRASP signal was denoted as cyan or yellow sphere automatically. When the cyan and yellow eGRASP signals overlapped in a single synapse, it was denoted as a yellow spot as the presynaptic neuron of the synapse indicating IEG-positive during memory formation. Also, if a dendrite did not have any cyan eGRASP or if the myr_mScarlet-I and myr_iRFP670 signal overlapped in a single dendrite, the dendrite was not denoted as a filament for more accurate analysis.

For eGRASP density analysis, the numbers of denoted cyan and yellow spheres were manually counted along each denoted filaments. The length of each

dendrite was measured using Imaris FilamentTracer. Cyan and yellow eGRASP density of each dendrite were normalized to the average density of the cyan and yellow eGRASP on the myr_iRFP670-positive dendrites, respectively, in each image. After denoting the trackable dendrites and eGRASP signals in the same way, eGRASP signal positive spines on denoted dendrites were reconstructed as 3D models and were measured using Imaris FilamentTracer. The investigator who reconstructed the spine 3D models was unaware of the color of the eGRASP signals.

Statistical analysis

Data were analyzed using Prism software. Mann Whitney two-tailed test and Tukey's multiple comparison tests after one-way ANOVA were used to test for statistical significance when applicable. The exact value of n and statistical significance are reported in each figure legends.

RESULTS (collaborated with Ji-il Kim)

Strategy for labeling the four possible synaptic connections between CA3 and CA1 at different strength of fear memory

To compare synaptic engram (E-E) synapses between different strength of memory group, fist I distinguish the four kinds of synapse in hippocampus CA3 to CA1, after fear conditioning. I used the same combination of AAVs and behavior protocol as described in Chapter II (Fig. 6), and injected virus in CA3 and CA1. To label synaptic engram, I expressed post-eGRASP with membrane targeting myristoylated mScarlet-I unilaterally in CA1 engram cells. Meanwhile, yellow pre-eGRASP was expressed in the contralateral CA3 engram cells to avoid possible coexpression of pre-eGRASP and post-eGRASP construct in a neuron. Then, E-E synapses could be identified as yellow eGRASP signals on mScarlet-I labeled dendritic spines. In addition, I expressed post-eGRASP together with myristoylated iRFP670 in a sparse neuronal population from the ipsilateral CA1. For strong expression in random population of neurons, I injected a high titer of EF1α promoter-driven Double-floxed Inverted cyan pre-eGRASP AAV construct with a lower titer of CaMKIIα promoter-driven iCre recombinase expressing AAV. In this strategy, I achieved strong expression in the random, sparse neuronal population using a high titer of Double-floxed Inverted open reading frame (DIO) AAV with a lower titer of Cre recombinase expressing AAV.

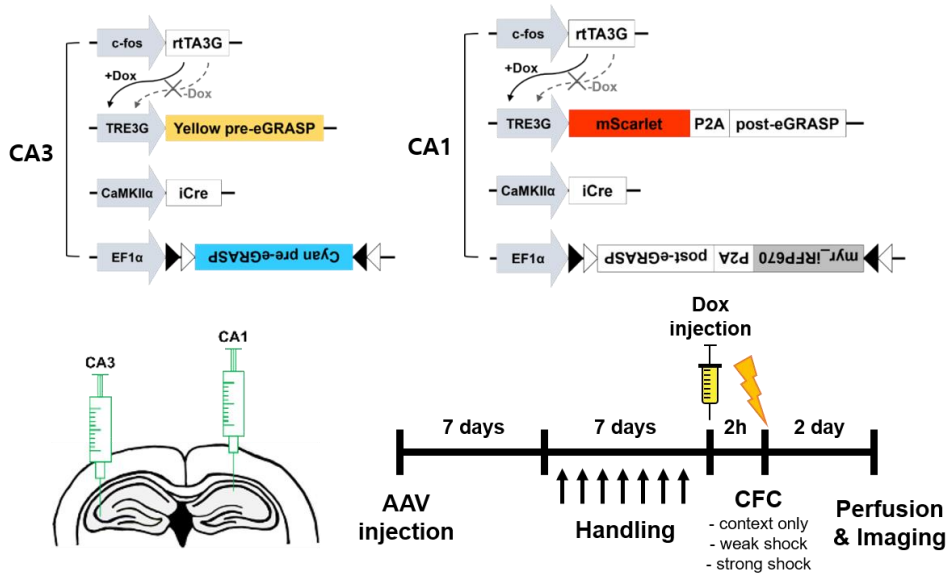

Figure 11. Strategy of labeling the synaptic engram in hippocampus.

Schematic illustration of injected viral combinations and injection sites. Pipeline of the experimental protocol.

Number of engram cells remain constant across different memory strength

I predicted that connectivity between pre- and post-engram cells could encode memory strength. To induce different strengths of memory, we randomly divided mice into three groups: weak, strong and context only. Mice were exposed to either a weak (one shock of 0.35mA) or strong (three shocks of 0.75mA) electric foot shocks during CFC, while mice in the context only group were exposed in the context without any electric foot shocks (Fig. 12A). Increasing electric foot shock intensity during memory formation produced a stronger freezing response (Fig. 12B). When we quantified the number of CA3 and CA1 engram cells, we found no significant differences among the three groups consistent with a previous report (Morrison et al., 2016) (Fig. 13 A,B).

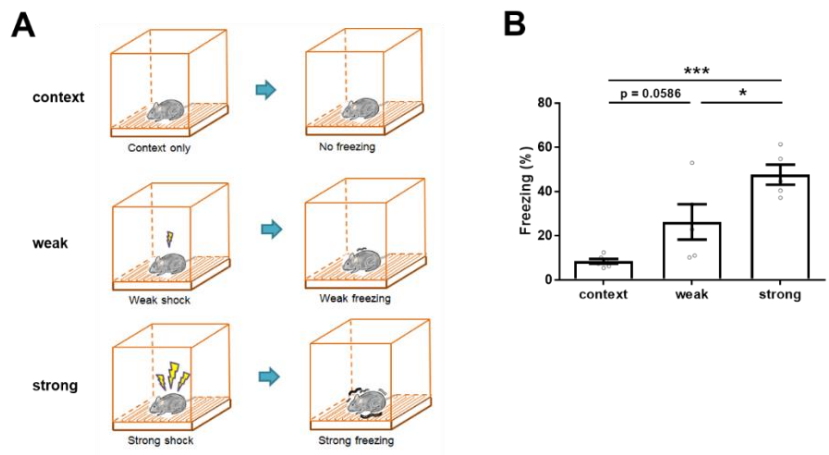

Figure 12. Increasing electric foot shock intensity during memory formation produced higher freezing levels.

(A) Schematic illustration of the conditioning and retrieval process

(B) Freezing levels for each group: context, n = 6; weak, n = 5; strong, n = 5, Tukey's multiple comparison test after one-way ANOVA; $F(2,13) = 15.85$, $^{*}p < 0.05$, $^{***}p < 0.001$.

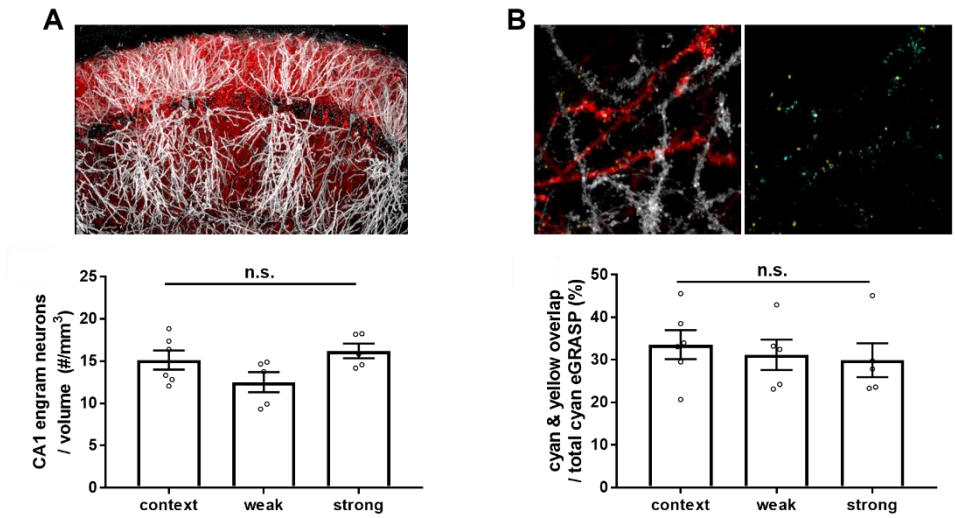

Figure 13. Comparable number of CA3 and CA1 engram cells across the different memory strength.

(A) (Top) Representative images of expressed CA1 engram and non engram neurons. (Bottom) The number of CA1 engram neurons expressing myr_mScarlet-I was constant among three groups. context, n = 6; weak, n = 5; strong, n = 5, one-way ANOVA, n.s.: not significant, $F(2,13) = 2.872$, $p = 0.0927$.

(B) (Top) Representative images of cyan and yellow eGRASP signals on CA1 dendrite. (Bottom) The number of CA3 engram neurons estimated through the percentage of yellow eGRASP signal overlapping on cyan eGRASP signal was constant among three groups. context, n = 6; weak, n = 5; strong, n = 5. one-way ANOVA, n.s.: not significant, $F(2,13) = 0.264$, $p = 0.7720$. Data are represented as mean ± SEM.

Reconstruction of eGRASP signals on hippocampal CA1 dendrites using IMARIS program

For quantitative analyzing of eGRASP signals on engram and non-engram dendrites, I used IMARIS 3D modeling programs. Each mScarlet-I-positive or iRFP670-positive dendrite was marked as a filament manually while hiding other fluorescent signals to exclude any bias, and each cyan or yellow eGRASP signal was marked as cyan or yellow sphere through automatic detection, respectively. I considered overlapped cyan and yellow eGRASP signals as yellow signal. I ruled out the dendrites without any cyan eGRASP or mScarlet-I, iRFP670-overlapping dendrites for more precise analysis (Fig. 14).

After 3D reconstruction of images, I measure the synaptic density and morphological properties of dendritic spines. The numbers of denoted cyan and yellow eGRASP signals along in each denoted dendrite filaments were counted manually. Spines of designated mScarlet-I-positive and iRFP670-positive dendrites were manually reconstructed with automatic detection of diameter and volume. Spine head diameter, spine head volume, and spine length were automatically measured with Imaris FilamentTracer.

Synaptic connectivity between pre- and post-engram cells is correlated to memory strength.

If synaptic connectivity between engram neurons, not the actual number of neurons, is the critical parameter for memory strength, the strong group should have a greater number of synapses among engram neurons compared to the other groups. I have analyzed cyan and yellow eGRASP signals on CA1 pyramidal neurons originating from pre synaptic CA3 cells. There were no significant differences between the density of N-N and N-E synapses, cyan eGRASP, in all groups (Fig. 15A). However, we found a significantly higher density of E-E synapses, yellow eGRASP, in the strong shock group compared to the context only and weak shock group (Fig. 15B). We further investigated whether the size of spines was positively correlated with memory strength. Spine head diameter and spine volume of E-E synapse, synaptic engram, were significantly greater in the strong shock group than in the other groups (Fig. 16B), whereas N-N and E-N did not show any significant differences in all groups (Fig. 16A). Collectively, these data suggested that memory strength while the connectivity is significantly enhanced with a stronger memory (Fig. 17).

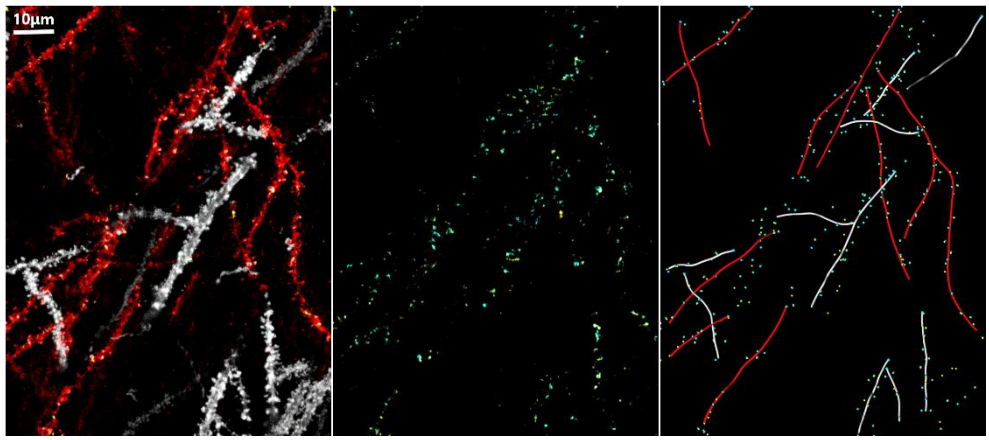

Figure 14. Representative images with 3D modeling for analysis.

Dendrites of CA1 engram or non-engram cells were labeled by myr_mScarlet-I or myr_iRFP670, respectively. Each dendrite was reconstructed as 3D filament. Synapses input from CA3 engram cells were labeled by yellow eGRASP signal, and cyan eGRASP signals came from random populations of CA3 neurons. Each eGRASP signal was denoted as 3D sphere.

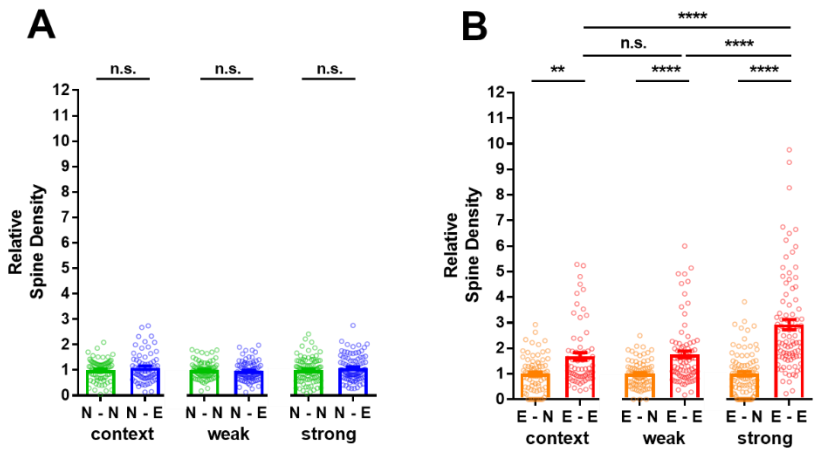

Figure 15. Synaptic density between pre- and post-engram cells is correlated to memory strength.

(A) Comparable relative spine density between N-N and N-E in all groups. (B) Synaptic density of each connection between E-N and E-E in all groups. (A and B) n = 74, context N-N; n = 67, context N-E; n =79, weak N-N; n = 80, weak N-E; n = 92, strong N-N; n = 91, strong N-E; n = 74, context E-N; n = 67, context E-E; n = 79, weak E–E; n = 80, weak E-N; n = 92, strong E-E; n = 91, strong E-N. 15 images from 6 mice for context group. 16 images from 5 mice for weak group. 19 images from 5 mice for strong group. Mann Whitney two-tailed test, n.s.: not significant, *p < 0.05, **p < 0.01, ***p < 0.001, ****p < 0.0001.

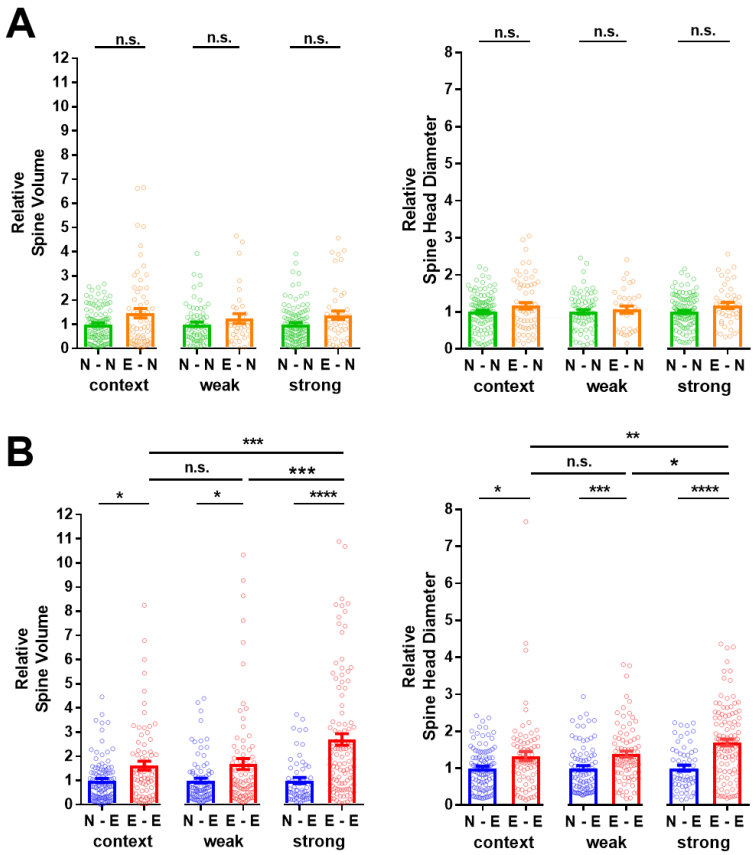

Figure. 16. Spine size of synaptic engram is correlated to strength of memory.

(A) (Left) Comparable spine volume and (Right) spine hed diameter between N-N spines and E-N spines in all groups. (B) The degree of enhancement of spine volume and spine head diameter for E-E spines by conditioning is significantly higher in strong group than that in weak and context groups. (A and B) Each data point represents a spine. n = 107, context N-N; n = 64, context E-N; n = 72, weak N-N; n = 34, weak E-N; n = 112, strong N-N; n = 46, strong E-N; n = 103, context N-E; n = 77, context E-E; n = 85, weak N-E; n = 84, weak E-E; n = 57, strong N-E; n = 110, strong E-E, 6 mice for context group, 5 mice for weak group, 5 mice for strong group.

Mann Whitney two-tailed test, n.s.: not significant, *p < 0.05, **p < 0.01, ***p < 0.001, ****p < 0.0001. Data are represented as mean ± SEM.

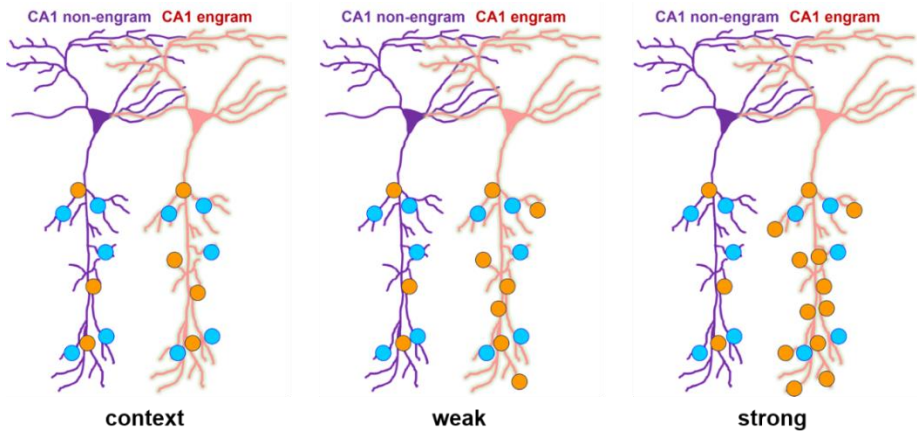

Figure. 17. Collective illustration of synaptic engram representing the strength of memory.

Schematic illustrations of hypothesized results showing higher density of E-E synapses with increasing memory strength.

DISCUSSION

In the previous chapter, I distinguished the four possible synapses among hippocampal CA3 to CA1, shaffercolateral pathway. Tripartite synaptic pathway in the hippocampus is well known for processing of contextual information. My previous study demonstrated that CA3 to CA1 connection between engram cell shows increased structural connectivity, but not detected in synapses between other connections. It indicates, synaptic populations that fired together during memory acquisition showed stronger connections demonstrates that classical Hebbian plasticity indeed occurs during learning and memory process among engram synapses (Andersen et al., 2017; Hebb, 1949).

I proposed that cells with higher connectivity are allocated together into a memory circuit, in contrast to enhanced connectivity after learning. However, the number of engram cells remains constant regardless of the different intensity of fear response. Through this interesting phenomena, I had raised the question, “Which mechanism attribute to the strength of memory?”. I found a significantly increased density and spine size of synaptic engram (E-E synapses) in the strong memory group compared to the weak memory groups. The relationship between memory strength and synaptic connectivity suggests that these specific connections between engram cells across two directly connected brain regions form the synaptic substrate for memory. In the other word, synaptic engram represents the strength of our memory (Choi et al., 2018).

CHAPTER IV

Synaptic engram represents the state of fear memory;

Conditioning, Extinction and Re-conditioning

INTRODUCTION

Successful adaptation to the environment requires making accurate responses to external threats, followed by encoding and retrieving these experiences. The utility of these responses can be shaped by using fear extinction, a well-established behavioral paradigm that can reveal the underlying neural processes. Fear extinction pairs repeated exposure to a conditioned stimulus (CS) without an aversive unconditioned stimulus (US), which gradually diminishes the encoded fear response. This extinction process facilitates survival by reducing unnecessary energy consumption (Maren, 2001; Pavlov, 1927; Quirk and Mueller, 2008) and refines vital behavioral responses. These innate fear acquisition and extinction processes are well defined in auditory fear conditioning paradigms, which rely on an auditory cortex (AC) to lateral amygdala (LA) circuit to establish and recall auditory fear memories (Duvarci and Pare, 2014; Kwon et al., 2014).

While the physiological changes induced by fear learning and extinction are well-known, the underlying synaptic correlates that mediate extinction remain unclear. Two mechanisms are currently proposed to drive extinction: unlearning and new learning. In the unlearning hypothesis, extinction reverses the changes induced by fear conditioning (An et al., 2017; Rich et al., 2019). In contrast, the new learning hypothesis contends that extinction occurs when newly formed non-aversive information overrides previously formed fear memory (Lacagnina et al., 2019; Myers and Davis, 2007). However, evidence to support one mechanism over the other remains limited.

In the previous chapter II, I used dual-eGRASP combined with a c-fos promoter driven labeling system, and labeled synapses between cortico-amygdala engram neurons and compared the four possible synapses and identified the synaptic engram after fear learning. In this chapter, using same genetic strategies mentioned above, labeled the synaptic engrams in lateral amygdala and compared the morphological dynamics after fear learning, extinction and re-conditioning to prove the synaptic engram is altered by state of memory.

EXPERIMENTAL PROCEDURES

Animals

All experiments were performed on 8~10-week-old male C57BL/6N mice purchased from Samtako. Bio. Korea. Mice were raised in 12-hr light/dark cycle in standard laboratory cages and given ad libitum access to food and water. All procedures and animal care followed the regulation and guidelines of the Institutional Animal Care and Use Committees (IACUC) of Seoul National University.

AAV production

We produced Adeno-Associated Viruses serotype 1/2 (AAV1/2; AAV particle that contains both serotype 1 and 2 capsids) as described in our previous study. Briefly, AAV1/2s were purified from HEK293T cells that were transfected with plasmids containing each expression cassette flaked by AAV2 ITRs, p5E18, p5E18-RXC1 and pAd-ΔF6 and cultured in 18 ml or 8 ml Opti-MEM (Gibco-BRL/Invitrogen, cat# 31985070) in a 150-mm or 100-mm culture dish, respectively. Three to four days after transfection, the medium was collected and centrifuged at 3,000 rpm, 10 min. After 1 ml of heparin-agarose suspension (Sigma, cat# H6508) was loaded onto a poly prep chromatography column (Bio-Rad Laboratories, Inc. cat# 731-1550), the supernatant was loaded onto the column carefully. The column was washed by 4 ml of Buffer 4-150 (150 mM NaCl, pH4 10 mM citrate buffer) and

12 ml of Buffer 4-400 (400 mM NaCl, pH4 10 mM citrate buffer). The virus particles were eluted by 4 ml of Buffer 4-1200 (1.2 M NaCl, pH4 10 mM citrate buffer). The eluted solution was exchanged with PBS and concentrated using an Amicon Ultra-15 centrifugal filter unit (Millipore, cat# UFC910024). The titer was measured using quantitative RT-PCR.

Stereotaxic surgery

Mice (8~10 weeks) were anaesthetized with a ketamine/xylazine solution and positioned on a stereotaxic apparatus (Stoelting Co.). The virus mixture was injected into target regions through 32gauge needle with Hamilton syringe at a rate of 0.125 μl/min. Total injection volume per each sites was 0.5 μl, and a tip of the needle was positioned 0.05 mm below the target coordinate right before the injection for 2 minutes. After the injection was completed, the needle stayed in place for extra 7 minutes and was withdrawn slowly. Stereotaxic coordinates for each target sites were: auditory cortex (AP: -2.9/ ML: ±4.5/ DV: -3.2), auditory thalamus (AP: -3.1/ ML: ±1.8/ DV: -3.6), and lateral amygdala (AP: -1.45/ ML: ±3.4/ DV: -4.4).

0.5 μl of a mixture of viruses ($1.5x10^8$ viral genome (vg)/μl of Fos-rtTA3G, $8.0x10^8$ vg/μl of TRE3G-Yellow pre-eGRASP, $1.5x10^7$ vg/μl of CaMKIIα-iCre, and $4.0x10^8$ vg/μl of EF1α-DIO-Cyan pre-eGRASP) was injected into auditory cortex or auditory thalamus. 0.5 μl of a mixture of viruses ($1.5x10^8$ vg/μl of Fos-rtTA3G, $7.0x10^8$ vg/μl of TRE3G-myr_mScarlet-I-P2A-post-eGRASP, $7.0x10^5$ vg/μl of CaMKIIα-iCre, $4.0x10^8$ vg/μl of EF1α-DIO-myr_iRFP670-P2A-post-eGRASP) was injected into lateral amygdala.

Auditory fear conditioning

All mice were fear conditioned 2 weeks after the AAV injection. Each mouse was single caged 10 days before conditioning and was habituated to the hands of the investigator and anesthesia chamber without isoflurane for 7 consecutive days. In all experiments, fear conditioning and extinction took place in two different contexts (context A and context B) to minimize the influence of contextual associations. Context A consist of a square chamber with steel grid floor (Coulbourn instruments; H10-11M-TC), and context B consist of a rectangular plastic box with a striped walls and a hardwood laboratory bedding (Beta chip). 2 hours prior to the conditioning, 250 μl of 5 mg/ml Doxycycline solution dissolved in saline was injected intraperitoneally during brief anesthesia by isoflurane. For auditory fear conditioning, mice were placed in the context A and allowed to explore the context for 150 seconds, followed by three exposures to auditory tone CS (30 sec), each of which coterminated with 2 seconds, 0.75mA footshock US, with a 30 sec inter-trial interval. After the conditioning, mice were immediately delivered to their homecages. 1 day after the conditioning, mice were placed into a novel context B and exposed to the auditory tone to measure the freezing behavior. The freezing behavior was recorded and scored using video-based FreezeFrame fear-conditioning system.

Fear extinction and re-conditioning

Mice were divided into control group and extinction group. For three consecutive days, mice of extinction group were placed into context B, and after 2 minutes of exploration period, the auditory tone was administered 20 times with 30 seconds inter-trial interval in the absence of the footshock. Mice of control group

stayed in their homecage during the extinction session. 1 day after the last extinction session, mice were placed into context B and exposed to the auditory CS to measure the freezing behavior.

For re-conditioning, fear-extinct mice were separated into an extinction group and a re-conditioning group. Mice in the re-conditioning group were re-conditioned under identical conditions as the original auditory fear conditioning procedure. Mice in the extinction group stayed in their homecage during the re-conditioning session. The measurement of freezing behavior was identical to the original procedure.

Sample preparation and confocal imaging

Perfused brains were fixed with 4% paraformaldehyde in phosphate buffered saline (PBS) overnight at 4℃, and dehydrated in 30% sucrose in PBS for 2 days at 4℃. Brains were sliced by Cryostat into 50 μm section for dual-eGRASP analysis and 40 μm section for immunohistochemistry. Sections were mounted in VECTASHIELD mounting medium (Vector Laboratories). For dual-eGRASP analysis, LA dendrites were imaged in Z-stack by Leica SP8 confocal microscope with 63x objective with distilled water immersion. For c-fos analysis, IHC samples were imaged in Z-stack by SP8 confocal microscope with 20x objective.

Immunohistochemistry

40μm sections were rinsed three time in 1x PBS. Sections were blocked for 1hr at room temperature in 1x PBS with goat serum. Sections were incubated in rabbit anti-c-fos(Synaptic systems; 226003; 1:1,000), primary antibody were

dissolved in the blocking solution, incubated at 4'C for 16h. After incubation, sections were rinsed three time for 5min in 1x PBS. Sections were incubated in secondary antibody (ThermoFisher, goat anti-rabbit 647, 1:500) for 2h at room temperature followed by three time rinsed with 1x PBS.

Image analysis

Processing of confocal image and 3D reconstruction of dendrites were performed using Imaris (Bitplane, Zurich, Switzerland) software. Each mScarlet-I-positive or iRFP670-positive dendrite was marked as a filament manually while hiding other fluorescent signals to exclude any bias, and each cyan or yellow eGRASP signal was marked as cyan or yellow sphere through automatic detection. Overlap of cyan and yellow eGRASP signals was considered as yellow signal since the presynaptic neuron of the synapse is c-fos-positive during memory formation. Dendrites without any cyan eGRASP or mScarlet-I, iRFP670-overlapping dendrites were ruled out for more precise analysis.

Spines of designated mScarlet-I-positive and iRFP670-positive dendrites were manually reconstructed with automatic detection of diameter and volume. Each spine was defined as an engram or non-engram spine depending on its presence of yellow or cyan eGRASP signal through manual detection. Spine head diameter, spine head volume, and spine length were measured with Imaris FilamentTracer. The examiner was unaware of any eGRASP signals during reconstruction of the spine 3D models. The number of eGRASP signals were counted manually by the investigator unaware of mice group.

RESULTS **(Collaborated with Ji-il Kim)**

Labeling four types of synapses between engram and non-engram neurons after fear conditioning and extinction.

Using dual-eGRASP combined with a c-f-os promoter driven labeling system, I labeled synapses between cortico-amygdala engram neurons and compared the morphological dynamics after fear learning and extinction. To mark the specific synaptic inputs from presynaptic engram neurons, I used a same combination of AAVs and Fos promoter driven engram labeling strategy as described in chapter II (Fig. 18)(Choi et al., 2018; Choi et al., 2014). Two weeks after viral inject in auditory cortex and lateral amygdala, auditory fear conditioning was conducted.

After auditory fear conditioning, I divided the mice into an extinction and a control group. The control group remained in their homecages, while the extinction group was exposed to the same tone without electric foot shock for three days (Fig. 19A, B). The series of tone exposures decreased fear responding in the extinction group compared to conditioning group (Fig. 19C).

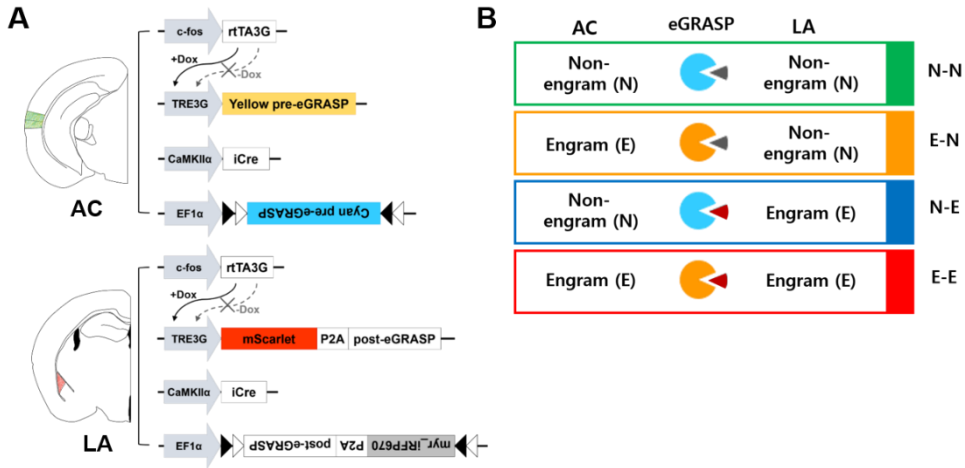

Figure 18. Strategy of labeling the synaptic engram in lateral amygdala.

(A) Schematic illustration of injected viral combinations and injection sites. (B) Classification of the four synaptic populations.

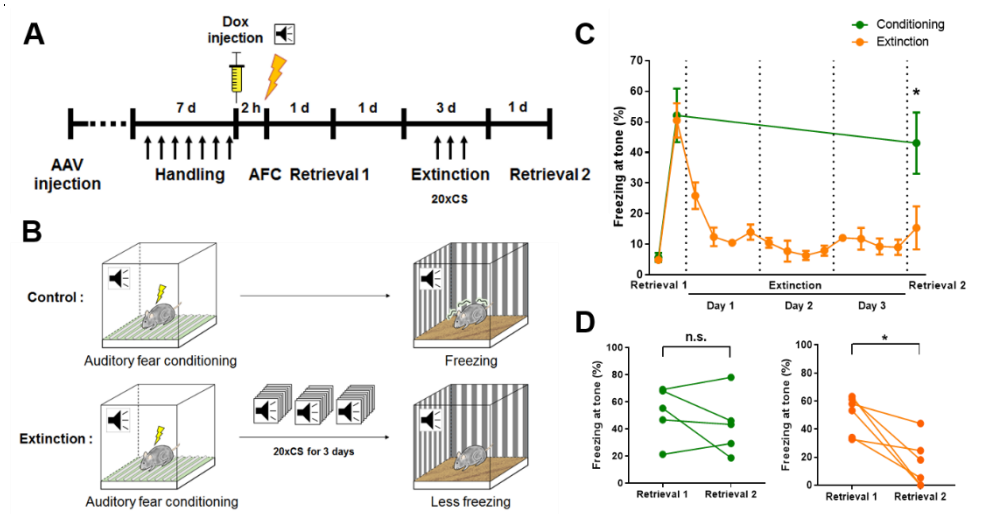

Figure 19. Fear extinction decreased the tone induced fear response.

(A) Experimental protocol.

(B) Schematic illustrations of the conditioning and extinction processes. Mice were placed into either the control or extinction groups. Both groups were conditioned to an auditory tone. Mice in the extinction group were repeatedly exposed to the tone, while mice in the control group remained their homecages.

(C) Freezing levels for each group. Each data point represents the average of freezing levels during 5 minutes. Control, n=5; Extinction, n=7; Unpaired t test of freezing levels at retrieval 2; *P = 0.0453.

(D) (Left) Freezing level of mice in control group were constant across twice retrieval in different time points. (Right) Freezing levels of mice in the extinction group decreased after extinction, control, n = 5; extinction, n =7. Paired t test within each group, n.s. = not significant, *P = 0.0113

Successful discrimination of the four possible synapses between auditory cortex and lateral amygdala using dual-eGRASP

After our behavioral paradigm, I could clearly distinguish all four types of synapses between AC to LA connections within the same brain slice from both control and extinction groups. Based on these results, I concluded that the spines with only cyan eGRASP signal represented synapses receiving input from auditory cortex non-engram neurons, whereas the spines with yellow eGRASP signal indicated the connections from engram neurons. AC engram to LA engram (E-E) synapses were labeled with yellow eGRASP signals on mScarlet-I-positive dendrites, while non-engram to engram synapses (N-E) were labeled with cyan eGRASP signals on mScarlet-I-positive dendrites. Likewise, engram to non-engram (E-N) and non-engram to non-engram (N-N) synapses were marked by yellow and cyan eGRASP signals on iRFP670-positive dendrites, respectively. These eGRASP signals remained stable until the completion of all behavioral tasks (Fig. 20).

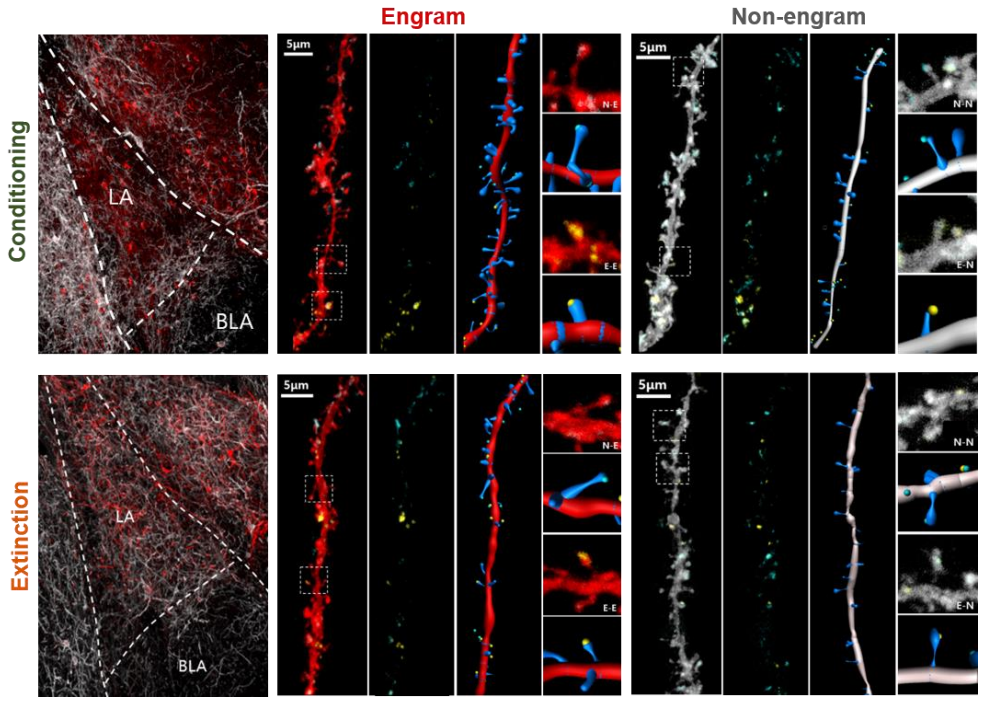

Figure 20. Representative images with 3D modeling for analysis in lateral amygdala engram and non-engram dendrites after extinction.

Dendrites of lateral amygdala engram or non-engram cells were labeled by myr_mScarlet-I or myr_iRFP670, respectively. (Top) conditioning group (Bottom) extinction group. Each dendrites were reconstructed as 3D filaments using IMRAIS. Synapses input from auditory cortex engram cells were labeled by yellow eGRASP signal, and cyan eGRASP signals came from random populations of auditory cortex neurons. Each eGRASP signal was denoted as a 3D sphere using IMRAIS.

Extinction reversed the fear conditioning induced enhancement of spine head size of synaptic engram.

I investigated whether different memory state correlates with size of synaptic engrams using the same combination of AAVs and strategy as described in chapter II. I measured and analyzed parameters corresponding to spine morphology at each type of synapse. I found a significant increase in spine head diameter and volume at E-E synapses after fear conditioning compared to N-E synapses. In contrast, E-N and N-N synapses did not show any significant differences (Fig. 21). These results are consistent with my previous study that showed synapses between engram neurons in CA3 to CA1 circuits are selectively enhanced during fear memory encoding (Choi et al., 2018). Surprisingly, extinction reversed this enhanced spine head size at E-E synapses (Fig. 21A) but did not modify the relative head size of E-N synapses compared to N-N synapses (Fig. 21B). Based on these results revealed that extinction reversed the synaptic enhancement induced by fear conditioning.

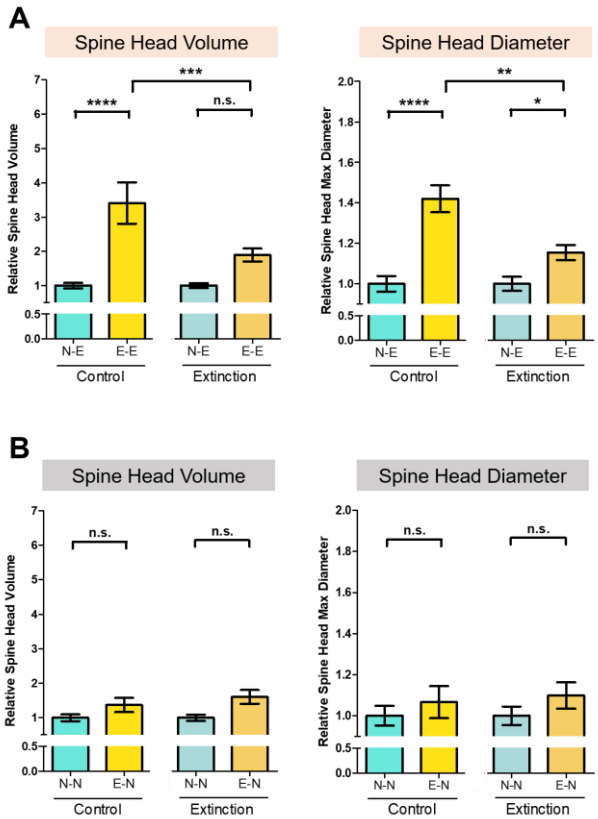

Figure 21. Extinction reversed the fear conditioning induced enhancement of spine head size of E-E synapses.

(A) and (B), Normalized head diameter, head volume, and length of spines on dendrites from engram (A) and non-engram (B) lateral amygdala neurons. Parameters of spines with yellow puncta were normalized to those of the spines with cyan-only puncta of the same dendrite. n = 113, control N-E; n = 242, control E-E; n = 140, extinction N-E; n = 271, extinction E-E, n = 92, control N-N; n = 45, control E-N; n = 97, extinction N-N; n = 87, extinction E-N. Control group, n=3-5; Extinction group, n=4-. Mann Whitney two-tailed test, n.s. = not significant. *P < 0.05, **P < 0.01, ***P < 0.001, ****P < 0.0001. Data are represented as mean ± SEM.

Re-conditioning increases the size of the synapse engram reduced by fear extinction

In previous experiment, I found that extinction reversed the spine head size of synaptic engram which encode the fear memory. Based on this result, I supposed that if the synaptic engram is essential component of specific memory, the spine size reduced by extinction will be revived by re-conditioning. To confirm it, I applied the same viral combination as used in extinction experiment.

After fear extinction, I divided the mice into an extinction and a re-conditioning group. The extinction group was remained in their homecages, while the re-conditioning group was exposed to the same tone and electric foot shock as given in fear conditioning for a day (Fig. 22A, B). The freezing response disappeared by fear extinction was restored by re-conditioning of fear memory. (Fig. 22C).

I measured and analyzed parameters corresponding to spine morphology at each type of synapse after retrieval 3. I confirmed a no significant differences in spine head diameter and size between E-E and N-E synapses in extinction group, as confirmed in previous experience. Surprisingly, I found that re-conditioning with the same tone and foot shock increase the size of the E-E spine, which was reduced by fear extinction (Fig. 23). These results indicate that the structure of the synaptic engram diminished by fear extinction was restored by re-conditioning (Fig. 24).

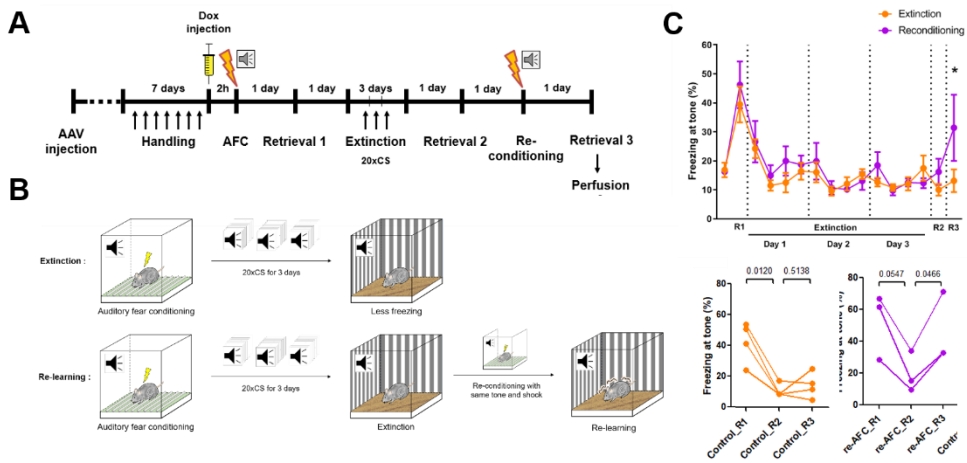

Figure 22. Re-conditioning with same tone and shock revived the extinct tone induced fear response.

(A) Experimental protocol.

(B) Schematic illustrations of the extinction and re-conditioning processes. Mice were placed into either the extinction or re-conditioning processes groups. Both groups were conditioned to an auditory tone. Mice in the extinction group were repeatedly exposed to the tone, while mice in the re-conditioning group exposed in same tone and shock, after fear extinction.

(C) (Top)Freezing levels for each group. Each data point represents the average of freezing levels during 5 minutes. Extinction, n=4; Re-conditioning, n=3; Unpaired t test of freezing levels at retrieval 3; *p = 0.0380. (Bottom, Left) Freezing level of mice in extinction group decreased after extinction in different time points. (Right) Freezing levels of mice in the re-conditioning group were increased after re-conditioning with same tone and shock, Extinction, n = 4; Re-conditioning, n =3. Paired t test within each group, n.s. = not significant, *p < 0.05.

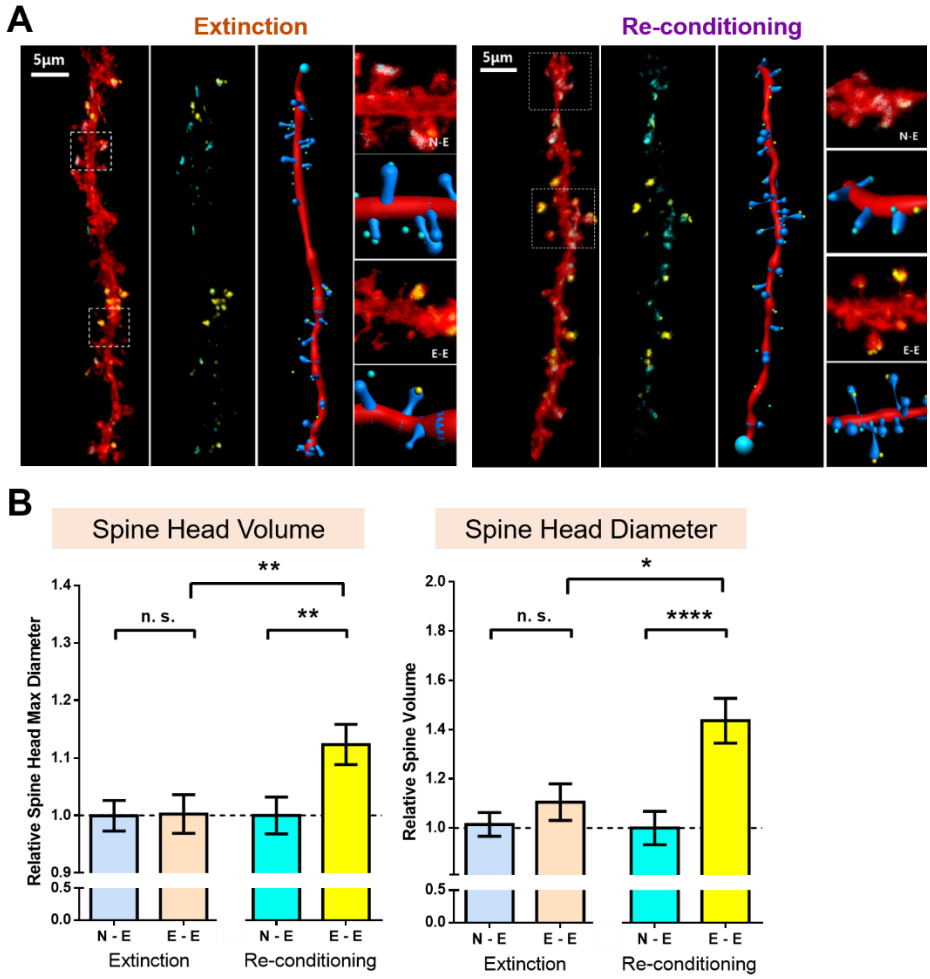

Figure 23. Re-conditioning increases the decreased spine head size of E-E synapses induced by fear extinction.

(A) Dendrites of lateral amygdala engram or non-engram cells were labeled by myr_mScarlet-I or myr_iRFP670, respectively. (Left) extinction group (Right) re-conditioning group.

(B) Normalized head diameter, head volume of spines on dendrites from engram lateral amygdala neurons. Parameters of spines with yellow puncta were normalized to those of the spines with cyan-only puncta of the same dendrite. n = 120, extinction

N-E; n = 76, extinction E-E; n = 109, re-conditioning N-E; n = 271, re-conditioning E-E, n = 87. Extinction group, n=4; Re-conditioning group, n=3. Mann Whitney two-tailed test, n.s. = not significant. *p < 0.05, **p < 0.01, ***p < 0.001, ****p 0.0001. Data are represented as mean ± SEM.

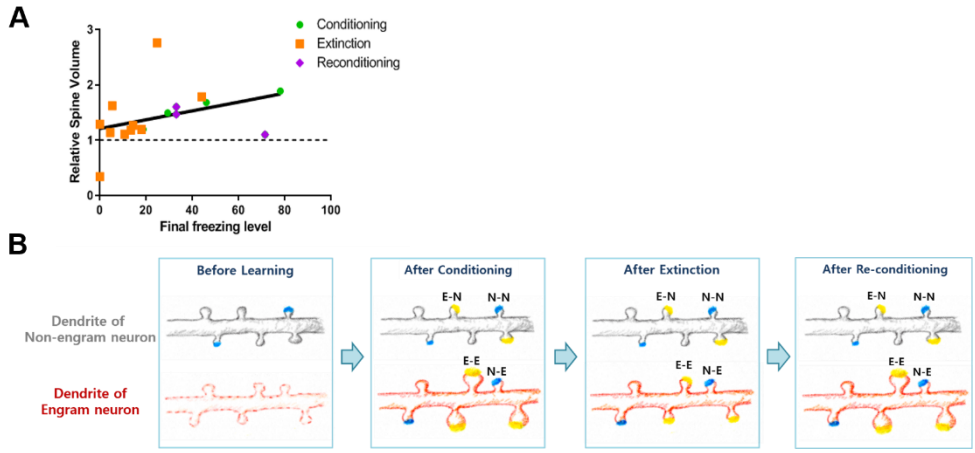

Figure 24. Synaptic engram represents the state of fear memory.

(A) Comparison between size of synaptic engram and freezing level of each group mice. Spine size and freezing level show correlation. Conditioning, n=4; extinction, n=10, re-conditioning, n=3. Pearson correlation test within total mice, *p < 0.05.

(B) Schematic illustrations representing dynamic changes of each type of synapses among engram and non-engram neurons in auditory cortex to lateral amygdala circuit by conditioning, extinction and re-conditioning.

DISCUSSION

Associated fear memory remain abidingly through whole life, because avoidance from external threats based on previous experience is crucial for survival of animal. Although its importance of surviving, no more fear response is elicited after extinction of fear memory. Since the enlargement of synapses between engram neurons is the key mechanism underlying memory encoding, the extinction mechanism of encoded memory is still remains controversial. Previous other studies could not directly examine changes at specific synapses that encode the auditory fear memory due to the lack of tools to trace engram-specific connections.

Likewise, in previous chapter, I employed our recently developed synapse labeling technique, dual-eGRASP, to investigate how extinction modified all four kinds of synapses within the AC to LA circuit after inducing an auditory fear memory. I posit these synapses are synaptic engrams, and traced it. Based on experimental results, I conclude that extinction reverses the enhancement at engram synapses, and re-conditioning restore the fear extinction induced synaptic engram decreasing.

Even though I provided the strong evidence of unlearning mechanism of fear extinction by analyzed structural properties between engram cells, accumulating studies also suggest that extinction recruit new engram neurons in BLA after extinction as new learning mechanism (Trouche et al., 2013). I cannot exclude that new learning can occur independently through a parallel process. The medial prefrontal cortex may develop an inhibitory circuit with the amygdala during memory extinction (Cho et al., 2013; Sotres-Bayon et al., 2004). Further studies will

delineate how these conflicting mechanisms in different brain regions function and integrate to mediate the expression of behavioral extinction. Overall, my experimental results provide evidence for the unlearning hypothesis, which postulates that extinction comprises a reversal of conditioning. Future studies will reveal whether my findings hold for other synapses in the fear learning circuit.

CHAPTER V

CONCLUSION

CONCLUSION

In this study, I identified the synaptic engram in hippocampus and amygdala, using recently developed synapse labeling daul-eGRASP technique. I could trace the physical evidence of memory at synaptic scale to demonstrate whether the synaptic engram represents the encoded memory.

In chapter II, I provided various examples of dual-eGRASP applying approaches. Dual-eGRASP could visualize the two different synaptic populations that originated from presynaptic neuronal ensembles. This technique could cover distinguish the projections from different brain region and cell type specific connections with cre-recombinase dependent manner. Most importantly, it can separate different properties of neurons, such as engram connections between different brain areas. Combining with fos promoter driven expression strategy, I had classified the four possible synaptic combinations: nonengram to engram (N-E), engram to nonengram (E-N), nonengram to nonengram (N-N) and engram to engram connections (E-E). The E-E connections are regarded as synaptic engrams. I successfully identified the synaptic engrams both in hippocampal CA3 to CA1 connections and cortico-amygdala connections, which are involved in encoding of fear memory.

In Chapter III, I labeled and analyzed the synaptic engrams of schaffercolateral pathway in hippocampus to confirm the difference in synaptic connections between engram cells according to memory intensity. I observed that the synaptic density and spine morphology of synapses between CA3 engram to CA1 engram cells are significantly strengthened after contextual memory formation. However, the allocated cell number remains constant regardless of the memory

strength, whereas the connectivity is significantly enhanced with a stronger memory. This finding indicates a significant contribution of post-learning enhancement over the predetermined connectivity.

In Chapter IV, I marked the synaptic engram of cortico-amygdala pathway in lateral amygdala and compared between different state of fear memory. I investigated how extinction and re-conditioning altered four kinds of synapses. Same like in hippocampus, I found a significant increase in spine head diameter and volume at E-E synapses, which is the synaptic engram, in lateral amygdala after fear conditioning. I found that extinction reversed this enhanced spine head size at E-E synapses but did not alter the relative head size of E-N synapses compared to N-N synapses. Furthermore, re-conditioning with same tone and shock revived the lost fear memory and re-enlarged the morphological characteristics which was reduced in synaptic engrams. Based on these results, I concluded that extinction and re-conditioning changes the synaptic enhancement induced by fear conditioning.

With advancements in technology, studies have identified and further have manipulate cells population that encode the memory, thereby revealing the physical trace of memory called engram. Furthermore, Donald O. Hebb's theory that “fire together, wire together” has been confirmed using a new technique, dual-eGRASP (Choi et al., 2018; Kim et al., 2012). The dual-eGRASP technique, which can selectively discriminate the connections among specific cells, has been able to show changes among engram cells and sheds light on the synaptic engram studies. In previous engram studies, optogenetic manipulation could induce selective weakening of connections originating from the presynaptic engram cells, and it could disappear the associated memory (Abdou et al., 2018; Rich et al., 2019).

However, experiments that specifically manipulate both the synaptic parts of the engram cells are still remained to be done. I expect that selective weakening of pre- and post-synaptic engram would erase the related memory. Furthermore, erased memory could be regenerated by enhancing the synaptic engram connections by applying LTP protocols. Synaptic changes are the fundamental principles of normal brain function. Therefore, defining synapses affected by various stimuli or diseases is critical for understanding the basis of behavioral changes.

Collectively, this study clearly revealed the importance and crucial role of synaptic engram which encode the specific memory. First, I found the correlation between size of synaptic engram and strength of memory. Second, I showed synaptic engram represents the different state of fear memory: conditioning, extinction and re-conditioning (Fig. 25). Indeed, I proved the physical evidence of memory in synaptic scale.

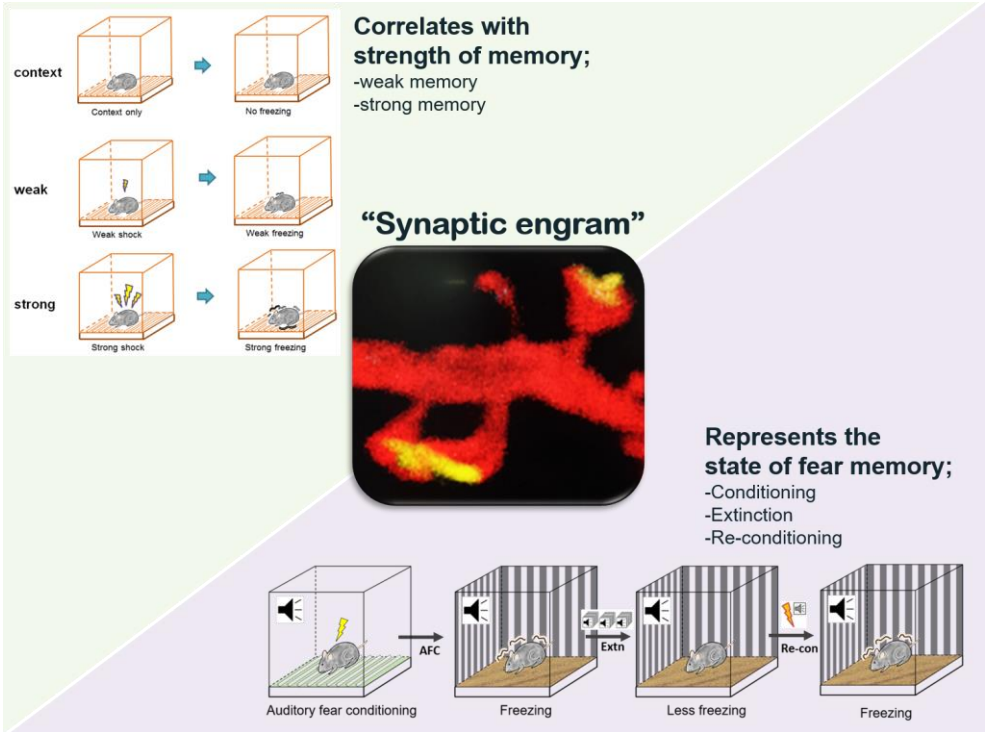

Figure 25. Synaptic engram, functional unit of memory, represents the state of memory.

Schematic illustration of synaptic engram thesis conclusion. The synaptic engram is correlated with strength of memory and state of fear memory.

REFERENCES

Abdou, K., Shehata, M., Choko, K., Nishizono, H., Matsuo, M., Muramatsu, S.-i., and Inokuchi, K.J.S. (2018). Synapse-specific representation of the identity of overlapping memory engrams. *360*, 1227-1231.

An, B., Kim, J., Park, K., Lee, S., Song, S., and Choi, S.J.E. (2017). Amount of fear extinction changes its underlying mechanisms. *6*, e25224.

Andersen, N., Krauth, N., and Nabavi, S. (2017). Hebbian plasticity in vivo: relevance and induction. Current opinion in neurobiology *45*, 188-192.

Bindels, D.S., Haarbosch, L., van Weeren, L., Postma, M., Wiese, K.E., Mastop, M., Aumonier, S., Gotthard, G., Royant, A., Hink, M.A*., et al.* (2017). mScarlet: a bright monomeric red fluorescent protein for cellular imaging. Nature Methods *14*, 53-56.

Chen, G., Zou, X., Watanabe, H., van Deursen, J.M., and Shen, J. (2010). CREB binding protein is required for both short-term and long-term memory formation. The Journal of neuroscience : the official journal of the Society for Neuroscience *30*, 13066-13077.

Cho, J.H., Deisseroth, K., and Bolshakov, V.Y. (2013). Synaptic encoding of fear extinction in mPFC-amygdala circuits. Neuron *80*, 1491-1507.

Choi, J.-H., Sim, S.-E., Kim, J.-i., Choi, D.I., Oh, J., Ye, S., Lee, J., Kim, T., Ko, H.-G., and Lim, C.-S.J.S. (2018). Interregional synaptic maps among engram cells underlie memory formation. *360*, 430-435.

Choi, J.-H., Yu, N.-K., Baek, G.-C., Bakes, J., Seo, D., Nam, H.J., Baek, S.H., Lim, C.-S., Lee, Y.-S., and Kaang, B.-K.J.M.b. (2014). Optimization of AAV expression cassettes to improve packaging capacity and transgene expression in neurons. *7*, 17.

Deng, W., Mayford, M., and Gage, F.H. (2013). Selection of distinct populations of dentate granule cells in response to inputs as a mechanism for pattern separation in mice. Elife *2*, e00312.

Duvarci, S., and Pare, D.J.N. (2014). Amygdala microcircuits controlling learned fear. *82*, 966-980.

Fanselow, M.S.J.B.b.r. (2000). Contextual fear, gestalt memories, and the hippocampus. *110*, 73-81.

Feinberg, E.H., Vanhoven, M.K., Bendesky, A., Wang, G., Fetter, R.D., Shen, K., and Bargmann, C.I. (2008). GFP Reconstitution Across Synaptic Partners (GRASP) defines cell contacts and synapses in living nervous systems. Neuron *57*, 353-363.

Gore, F., Schwartz, E.C., Brangers, B.C., Aladi, S., Stujenske, J.M., Likhtik, E., Russo, M.J., Gordon, J.A., Salzman, C.D., and Axel, R. (2015). Neural Representations of Unconditioned

Stimuli in Basolateral Amygdala Mediate Innate and Learned Responses. Cell *162*, 134-145.

Haasteren, G.v., Li, S., Ryser, S., and Schlegel, W. (2000). Essential Contribution of Intron Sequences to Ca2+-Dependent Activation of c-fos Transcription in Pituitary Cells. NEN *72*, 368-378.

Hayashi-Takagi, A., Yagishita, S., Nakamura, M., Shirai, F., Wu, Y.I., Loshbaugh, A.L., Kuhlman, B., Hahn, K.M., and Kasai, H. (2015). Labelling and optical erasure of synaptic memory traces in the motor cortex. Nature *525*, 333-338.

Hebb, D.O. (1949). The organization of behavior: A neuropsychological theory (New York, NY: Wiley).

Josselyn, S.A., Kohler, S., and Frankland, P.W. (2015). Finding the engram. Nat Rev Neurosci *16*, 521-534.

Josselyn, S.A., and Tonegawa, S. (2020). Memory engrams: Recalling the past and imagining the future. Science *367*.

Kim, J., Zhao, T., Petralia, R.S., Yu, Y., Peng, H., Myers, E., and Magee, J.C. (2011). mGRASP enables mapping mammalian synaptic connectivity with light microscopy. Nat Methods *9*, 96-102.

Kim, J., Zhao, T., Petralia, R.S., Yu, Y., Peng, H., Myers, E., and Magee, J.C.J.N.m. (2012). mGRASP enables mapping mammalian synaptic connectivity with light microscopy. *9*, 96-102.

Kwon, J.-T., Nakajima, R., Kim, H.-S., Jeong, Y., Augustine, G.J., Han, J.-H.J.L., and memory (2014). Optogenetic activation of presynaptic inputs in lateral amygdala forms associative fear memory. *21*, 627-633.

Lacagnina, A.F., Brockway, E.T., Crovetti, C.R., Shue, F., McCarty, M.J., Sattler, K.P., Lim, S.C., Santos, S.L., Denny, C.A., and Drew, M.R.J.N.n. (2019). Distinct hippocampal engrams control extinction and relapse of fear memory. *22*, 753.

Lamprecht, R., and LeDoux, J. (2004). Structural plasticity and memory. Nature reviews Neuroscience *5*, 45-54.

Leuner, B., Falduto, J., and Shors, T.J. (2003). Associative memory formation increases the observation of dendritic spines in the hippocampus. Journal of Neuroscience *23*, 659-665.

Liu, X., Ramirez, S., Pang, P.T., Puryear, C.B., Govindarajan, A., Deisseroth, K., and Tonegawa, S. (2012). Optogenetic stimulation of a hippocampal engram activates fear memory recall. Nature *484*, 381-385.

Loew, R., Heinz, N., Hampf, M., Bujard, H., and Gossen, M. (2010). Improved Tet-responsive promoters with minimized background expression. BMC Biotechnol *10*, 81.

Maren, S.J.A.r.o.n. (2001). Neurobiology of Pavlovian fear conditioning. *24*, 897-931.

Matsuzaki, M., Ellis-Davies, G.C., Nemoto, T., Miyashita, Y., Iino, M., and Kasai, H. (2001). Dendritic spine geometry is critical for AMPA receptor expression in hippocampal CA1 pyramidal neurons. Nat Neurosci *4*, 1086-1092.

Matsuzaki, M., Honkura, N., Ellis-Davies, G.C., and Kasai, H. (2004). Structural basis of long-term potentiation in single dendritic spines. Nature *429*, 761-766.

Minatohara, K., Akiyoshi, M., and Okuno, H. (2016). Role of immediate-early genes in synaptic plasticity and neuronal ensembles underlying the memory trace. Frontiers in molecular neuroscience *8*, 78.

Morrison, D.J., Rashid, A.J., Yiu, A.P., Yan, C., Frankland, P.W., and Josselyn, S.A. (2016). Parvalbumin Interneurons Constrain the Size of the Lateral Amygdala Engram. Neurobiology of learning and memory.

Myers, K.M., and Davis, M.J.M.p. (2007). Mechanisms of fear extinction. *12*, 120.

Pavlov, I.P. (1927). Conditional reflexes: an investigation of the physiological activity of the cerebral cortex.

Pignatelli, M., Ryan, T.J., Roy, D.S., Lovett, C., Smith, L.M., Muralidhar, S., and Tonegawa, S.J.N. (2019). Engram cell excitability state determines the efficacy of memory retrieval. *101*, 274-284. e275.

Quirk, G.J., and Mueller, D.J.N. (2008). Neural mechanisms of extinction learning and retrieval. *33*, 56.

Reijmers, L.G., Perkins, B.L., Matsuo, N., and Mayford, M. (2007). Localization of a stable neural correlate of associative memory. Science *317*, 1230-1233.

Rich, M.T., Huang, Y.H., and Torregrossa, M.M.J.C.r. (2019). Plasticity at thalamo-amygdala synapses regulates cocaine-cue memory formation and extinction. *26*, 1010-1020. e1015.

Ryan, T.J., Roy, D.S., Pignatelli, M., Arons, A., and Tonegawa, S. (2015). Engram cells retain memory under retrograde amnesia. Science *348*, 1007-1013.

Sanders, J., Cowansage, K., Baumgartel, K., and Mayford, M. (2012). Elimination of dendritic spines with long-term memory is specific to active circuits. Journal of Neuroscience *32*, 12570-12578.

Semon, R. (1921). The mneme (London, UK: G. Allen & Unwin).

Semon, R. (1923). Mnemic psychology (London, UK: G. Allen & Unwin).

Shcherbakova, D.M., and Verkhusha, V.V. (2013). Near-infrared fluorescent proteins for multicolor in vivo imaging. Nat Methods *10*, 751-754.

Sheng, M., and Greenberg, M.E. (1990). The regulation and function of c-fos and other immediate early genes in the nervous system. Neuron *4*, 477-485.

Sotres-Bayon, F., Bush, D.E., and LeDoux, J.E. (2004). Emotional perseveration: an update

on prefrontal-amygdala interactions in fear extinction. Learning & memory *11*, 525-535.

Tanaka, J.-i., Horiike, Y., Matsuzaki, M., Miyazaki, T., Ellis-Davies, G.C., and Kasai, H. (2008). Protein synthesis and neurotrophin-dependent structural plasticity of single dendritic spines. Science *319*, 1683-1687.

Trouche, S., Sasaki, J.M., Tu, T., and Reijmers, L.G. (2013). Fear extinction causes target-specific remodeling of perisomatic inhibitory synapses. Neuron *80*, 1054-1065.

Xie, H., Liu, Y., Zhu, Y., Ding, X., Yang, Y., and Guan, J.-S. (2014). In vivo imaging of immediate early gene expression reveals layer-specific memory traces in the mammalian brain. Proceedings of the National Academy of Sciences *111*, 2788-2793.

Zhou, X., Vink, M., Klaver, B., Berkhout, B., and Das, A.T. (2006). Optimization of the Tet-On system for regulated gene expression through viral evolution. Gene Ther *13*, 1382-1390.

국문초록

우리의 일상의 경험은 기억이라는 형태로 저장되어 한 개인을 정의하는 기반이 된다. 이러한 기억이 어떠한 메커니즘을 통해 우리의 뇌에 저장되는지는 인류의 오랜 관심사였다. 기억이 뇌에 저장되고 회상되는 과정에서 구조적 생리학적인 변화가 발생하며, 이것이 기억 저장의 물리적 실체인 앤그램이라 일컬어졌다. 기억형성과정동안 신경세포 사이의 연결부위인 시냅스에서는 변화가 일어나는데, 신경생물학자들은 특히 앤그램 세포(기억저장 세포) 연결 간의 변화에 초점을 맞추고자 하였다. 하지만 이전까지는 기술적인 한계로 인하여 시냅스 수준의 앤그램 세포 연구는 불가능했었다.

최근에 개발한 Dual-eGRASP 기술의 적용으로 앤그램 세포 사이의 연결 시냅스를 식별할 수 있게 되었으며, 이를 “Synaptic engram”이라고 정의하였다. 이번 연구를 통해 공포기억을 저장하고 있는 해마 및 편도의 synaptic engram을 표지 하여, 기억의 다양한 상태에 따른 변화를 추적 및 분석하였다. 해마의 하위 영역인 CA3 - CA1 사이 synaptic engram의 경우 기억의 세기에 따라서 연결의 세기가 증가한다는 것을 밝혀내었다. 청각 피질과 측면 편도 사이의 synaptic engram은 공포기억 형성에 의해서 연결이 강해지며, 공포의 소거 반응에 의해서 synaptic engram의 크기가 작아지는 것을 확인하였다. 더 나아가서 같은 학습으로 사라진 공포 기억을 되살리면, 공포 소거에 의해서 작아졌던 synaptic engram의 크기가 회복되는 것을 관찰하였다.

이러한 결과들을 바탕으로 기억을 저장하는 synaptic engram이 기억의 세기, 그리고 소거 및 재학습에 따른 행동의변화를 반영한다는 것을 확인하였다. 이 시냅스 단위의 앤그램 연구는 “기억이 우리 뇌에 어떻게 저장되는가” 를 설명하기 위한 지식 기반이 될 것이다.

.....

주요어 : 기억, 엔그램, 해마, 편도, 기억소거, Dual-eGRASP

학번 : 2015-22682